17
Copy
MEMO 3-16-59E

COPY 2

NASA MEMO 3-16-59E

NASA

MEMORANDUM

COMPARISON OF THREE NUCLEAR PROPULSION SYSTEMS FOR A LOGISTIC-TYPE AIRCRAFT

By Paul G. Johnson and Roger L. Smith

Lewis Research Center
Cleveland, Ohio

LIBRARY COPY

LEWIS LIBRARY, NASA
CLEVELAND, OHIO

CLASSIFIED DOCUMENT

This material contains information affecting the national defense of the United States within the meaning of the espionage laws, Title 18, U.S.C., Secs. 793 and 794, the transmission or revelation of which in any manner to an unauthorized person is prohibited by law.

NATIONAL AERONAUTICS AND SPACE ADMINISTRATION

WASHINGTON
March 19, 1959
Reclassified October 16, 1961

[redacted]

NATIONAL AERONAUTICS AND SPACE ADMINISTRATION

MEMORANDUM 3-16-59E

COMPARISON OF THREE NUCLEAR PROPULSION SYSTEMS FOR A LOGISTIC-TYPE AIRCRAFT*

By Paul G. Johnson and Roger L. Smith

E-196

SUMMARY

A comparison of three nuclear propulsion systems for large, medium-altitude aircraft is made in terms of payload capability at design point. Direct-air, lithium, and helium turbojet systems are analyzed. The logistic-type aircraft are 500,000 pounds in gross weight and designed to fly at an altitude of 35,000 feet in the Mach number range from 0.9 to 2.5. Payload estimates are presented for ranges of operating temperature. The lithium system has the highest performance for the effective-reactor-wall-temperature range 1500° to 1900° F, with the helium system a close second.

INTRODUCTION

The use of a nuclear propulsion system in a large, medium-altitude aircraft to attain the combination of large payload capability and great range has always been recognized as one of the most attractive applications of aircraft nuclear propulsion. Many combinations of cycle types and operating conditions are possible, and the selection of a best system is difficult because experience with such high-performance nuclear systems is very preliminary.

The study herein reported is a comparison of three nuclear propulsion systems for an application typified by the logistic carrier, based on assumptions and analysis methods which are believed to be as consistent and fair as possible in a study of this scope. The three nuclear

*Title, Unclassified.

[redacted]

[redacted]

turbojet propulsion systems are: (1) a direct-air system, (2) a liquid-metal system using lithium-7 as the reactor coolant, and (3) a helium system. The aircraft is specified to be 500,000 pounds in gross weight, designed to fly at an altitude of 35,000 feet, and equipped with a unit shield for the protection of crew and cargo. Results are presented in terms of payload capability at various Mach numbers from 0.9 to 2.5. Only design-point performance is presented, and the number of turbojet engines is allowed to vary.

It is not the intent of the study to determine which cycle is the best, because the maximum temperatures at which the systems can successfully operate are not known. Rather, the study indicates the performance which may be expected for selected temperature ranges. The actual payload values shown are intended primarily for comparison of systems. Methods and assumptions are explained herein, and the accuracy and consistency of the comparison has been improved over previously reported results. It should be emphasized that many of the assumptions are intentionally optimistic, especially operating temperatures, engine and shield weights, materials, and reactor power density.

E-196

DESCRIPTION OF SYSTEMS

Schematic diagrams of the three propulsion systems are shown in figure 1. In all the systems several turbojet engines are coupled to one reactor. The reactor is the heat source, and the heat is transferred to the air of the turbojet engines either directly or through lithium or helium intermediate loops.

The direct-air system is shown in figure 1(a). The air leaving the turbojet compressor is ducted to the reactor, heated in passing over the fuel elements, and ducted back to the turbine. The primary advantages and disadvantages of the direct-air system are also listed in figure 1(a). Although the air entering the reactor will be at a high pressure because of high flight Mach number and compressor pressure ratio, it is such a poor heat-transfer fluid that the reactor core will be relatively large. The reactor shield will be correspondingly heavy, especially when it is a unit shield. An obvious advantage of the direct-air system is simplicity. Another is the elimination of intermediate heat-transfer processes with consequent temperature drops and pumping losses, although pressure losses in the ducts amount to a pumping loss and the one temperature drop is relatively large. Attainment of high turbine-inlet temperature is limited primarily by oxidation of the fuel elements, so that the maximum reactor wall temperature is the critical temperature of the direct-air system.

The lithium system is shown in figure 1(b). The turbojet air is heated in a heat exchanger located between the compressor and turbine. The lithium circulates in a closed loop transporting the reactor heat to the engine heat exchanger. The pump to circulate the lithium is driven

[redacted]

by the turbojet shaft, but this arrangement is used for simplicity of analysis rather than proved superiority.

The assumption is made that the isotope separation of the lithium will be sufficient to make an intermediate heat exchanger unnecessary. The lithium will be so predominantly lithium-7 that the cross section of the mixture will be extremely low, and no activation problem will be encountered. Thus, the lithium which cools the reactor can be brought outside the shield without complicating the shielding problem.

E-196

Liquid metals are very good heat-transfer fluids, and lithium is the best of the lot thermodynamically. As a result, the reactor core of a liquid-metal system will be relatively small and the shield correspondingly light. Also, the temperature differences between the lithium and the reactor fuel elements or the heat-exchanger walls will be small. The major problem in any liquid-metal system is corrosion and mass transfer. Some recent experimental investigations of lithium containment indicate good compatibility with columbium at temperatures up to 1700° F. Unfortunately, columbium oxidizes very readily in air at this temperature and, thus, is not a good heat-exchanger material. Some type of bimetal construction will be necessary if this compatibility is to be utilized.

Figure 1(c) shows a schematic diagram of a propulsion system which uses high-pressure helium as the reactor coolant. The diagram is identical to that of the lithium system. The coolant fluid has changed, but it is still used only as a heat-transfer medium. Alternative helium systems using the gas as a working fluid with a helium turbine to drive an air compressor or fan are possible, but the turbomachinery weight becomes very large at supersonic flight speeds.

Because of the high pressure of the helium (about 2000 lb/sq in. abs) the lines and heat exchangers will be heavy, but this pressure is an optimum compromise between these high component weights and the shield weight, which goes down as the high pressure reduces the reactor core size.

The principal reason for using helium as the reactor coolant is that its chemical inertness allows operation at relatively high fuel-element temperatures. Although oxidation of the air side of the heat exchanger is as much of a problem as ever, the troublesome area has been removed from the reactor, so that the problem seems less formidable. Reactor fuel elements of molybdenum can be expected to withstand much higher temperatures than will result in an oxidation problem downstream in the heat exchanger. In this study the maximum and effective reactor-fuel-element temperatures are assumed to be 3500° and 3120° R, respectively. Thus, the critical temperature in the helium system is the maximum heat-exchanger metal temperature, either due to oxidation or stress-rupture. Helium is also a convenient coolant because it does not become radioactive. As in the lithium system, no intermediate heat exchanger is necessary.

[redacted]

The size of the reactor in the helium propulsion system will be almost as small as that in the lithium system because of the characteristics of the fluid. At 2000 pounds per square inch absolute the density of the helium entering the reactor is approximately equal to the density of the air entering the reactor of the direct-air system. Since helium has a specific heat nearly five times that of air, the required coolant volume in the reactor will be less by this factor at least.

Although lithium, by these criteria, is a great improvement over either air or helium, little further reduction in reactor size can be attained. Figure 2 shows the relationship between reactor diameter and reactor coolant volume. The curves are determined from criticality calculations without consideration of coolant type. The points plotted on the curves correspond to the optimum reactors for the three systems at Mach 2 and an altitude of 35,000 feet. At this condition the coolants remove about 800 megawatts of power from the reactor. Two conclusions can be drawn from figure 2: (1) at such a high reactor power the direct-air system will require either a very large reactor or more than one reactor with an associated shield weight penalty, and (2) at these conditions helium is nearly as effective as lithium in reducing reactor size and shield weight. It should also be noted that the very small reactors operating at about 800 megawatts will have power densities far above values currently believed practical. If an upper limit were placed on power density, the comparison of systems would show less divergence as is discussed later.

E-196

METHODS

The comparison of nuclear propulsion systems for a large, medium-altitude aircraft of the logistic type is made in terms of payload capability at various design points but constant gross weight. The aircraft is specified to be of 500,000-pound gross weight and designed to fly at a 35,000-foot altitude. Flight Mach number is varied from 0.9 to 2.5. The effect of altitude variation is also shown for one Mach number.

The performance of each of the systems will be a strong function of the temperature level at which the system can be operated. However, there has not been enough experience accumulated with any of the system types to allow a particular temperature to be called a limit with confidence. Consequently, the results of this study are presented for ranges of temperature for each of the systems.

When the reactor fuel-element temperature is the critical temperature in the system, as in the lithium and direct-air systems, the effect of nonuniform fuel or heat-transfer-surface distributions is neglected. Effective reactor wall temperature is used instead. If the temperature profiles cannot be flattened, the results presented herein will correspond to even higher temperatures.

[redacted]

Effects of variations in other parameters, such as aircraft lift-drag ratio and allowable dose rate, are included to illustrate the degree of sensitivity of nuclear aircraft to these debatable parameters.

The weight of aircraft shields, especially unit shields, is one of the greatest uncertainties in any study of this type. The shield weights used in this comparison are the result of a very simplified analysis which is shown to be in close agreement with certain specific shield designs. By this means, trends are taken into account without involving a lengthy, complex computation procedure not suited for such a study.

E-196

Briefly, the shield analysis involved a rough optimization of shield shaping to provide a dose rate of 0.5 rem/hr at 50 feet along the forward centerline of the reactor-shield assembly. The dose rate of 0.5 rem/hr was selected at the beginning of the study and now seems to be much higher than allowable. For the purposes of the comparison, however, the important point to mention is that the relative placement of systems would be unchanged by a reduction in dose rate. Instead, differences between systems would be accentuated.

The shield materials are lithium hydride and depleted uranium. Although the latter may not be feasible at present, it seems attractive for use in the not too distant future. No differences were considered between cycles except in terms of power and diameter. The presence of a particular coolant was neglected, and duct effects were assumed to cost nothing in weight. Should such effects be appreciable, the spread between cycles would probably be increased but in the same order.

The simplified analysis was based mainly on an air-scattering optimization. Capture gammas were not taken into account directly, but the comparison with results of a more detailed study indicates that no large discrepancies exist. Another simplification was the lumping of all gamma shielding in one layer. Actually, it would be split up into thermal shields and laminated gamma shields to attenuate capture gammas arising in the outer layers of the shield. Since capture gammas and gamma heating were not analyzed, these effects must be assumed to be taken into account in the source-strength assumption, which matched the results of the simplified analysis to the model shields.

A complete list of assumptions and equations used in the analysis (appendix C) is included in appendix B, but a few pertinent assumptions are listed below:

(1) Ratio of aircraft structure weight to gross weight, 0.3

(2) Maneuverability thrust margin at design point, 20 percent

(3) Aircraft lift-drag ratio at Mach 2, 6.6

[redacted]

(4) Engine weights and component efficiencies the same for all systems, except compressor pressure ratio, which is optimized where possible

(5) Sea-level static compressor pressure ratio limited to range 2.5 to 15

Such design parameters as compressor pressure ratio, coolant flow rate, heat-exchanger inlet Mach number, reactor diameter and length, and turbine inlet temperature are optimized where possible. A description of the optimization procedure is included in appendix D. (All symbols are defined in appendix A.)

E-196

It should be noted that values of reactor diameter and fuel-element equivalent diameter are based strictly on heat-transfer and pressure-drop calculations. As mentioned previously, the very small reactors operating at high power represent power densities as high as 3500 watts per cubic centimeter. If, for example, the lithium reactors could be no smaller than the helium reactors, the difference in performance shown in the following comparison would be cut about in half. The question of reactor-passage equivalent diameter is illustrated by a consideration of values of the Mach 2, medium-temperature design points:

System	Equivalent diameter, $d_{e,R}$, in.
Direct-air	0.11
Lithium	.17
Helium	.26

The values for all systems seem within reason.

It is shown in appendix C that an allowance for a pressure shell is provided in the shielding analysis. This shell was not actually designed to withstand particular values of pressure, nor was a gamma heating calculation included in the analysis. If there were a large weight penalty, it would probably work against the helium system most severely and the lithium system the least.

[redacted]

E-196

RESULTS AND DISCUSSION

Direct-Air System

The estimated performance of the direct-air system is first shown in terms of payload against critical temperature in figure 3(a). The critical temperature in both systems involving chemically active coolants, air and lithium, is the maximum reactor fuel-element temperature. Figure 3(a) is plotted in terms of effective reactor wall temperature, however, because the analysis does not include an estimate of the spread between maximum and effective fuel-element temperature. Keeping this difference small (to within a few hundred degrees) will be one of the most difficult design and development problems associated with the direct-air system, calling for careful control of power and coolant flow distributions.

For an effective reactor wall temperature of 2400° F, the direct-air system gives payloads of about 100,000 pounds at speeds up to Mach 2, but the payload values drop rapidly with temperatures below this level and at Mach numbers higher than 2. The large difference between performance at Mach 0.9 and at Mach 2 is the effect of a large difference in airflow, a factor of over 4.5. Since all the air must go through one reactor and remove a great amount of heat, the reactor size is enormous at high speeds. The shield is correspondingly heavy, accounting for the relatively low payloads even at temperatures currently considered optimistic.

Lithium System

A plot showing the performance of the lithium system is given in figure 3(b). Although the maximum reactor fuel-element temperature would be greater than the effective value plotted, the difference would be small because of the excellent heat-transfer characteristics of the liquid metal.

In contrast to the payloads of the direct-air system, the values shown for the lithium system are quite impressive. For effective reactor wall temperatures between 1500° and 1900° F, this system gives payloads of about 200,000 to 220,000 pounds at flight Mach numbers from subsonic to above 2.5. Although the corrosion temperature limit is lower than the oxidation limit of the air cycle, the lithium system benefits from small reactor size and low compressor pressure ratio. Thus, the slightly lower specific impulse can be compensated for by increased total airflow without much weight penalty because the engines are light and the shield weight is relatively insensitive to flow-area change. Also, with a very low compression ratio, the performance remains good up to high Mach numbers and down to low reactor wall temperatures.

[redacted]

Helium System

The performance of the helium system is shown in figure 3(c), a plot of payload against maximum heat-exchanger wall temperature. The payload values are not a great deal less than those for the lithium system for the temperature ranges illustrated. For maximum heat-exchanger wall temperatures between 1600° and 2000° F, the helium system gives payloads of about 170,000 to 190,000 pounds. In comparison with the lithium system, the helium-system reactors are not quite as small, and the turbojet compression ratios are not quite as low, but the turbine inlet temperatures are higher. Both the helium and lithium systems would optimize at compressor pressure ratios less than a sea-level static value of 2.5 at Mach numbers of 2 or above, but they were limited to this value. This limit is slightly to the advantage of the helium system because the lithium system compressor pressure ratio is limited at Mach numbers as low as 1.5.

An interesting result of the optimization of the helium system is that the best compromise between helium pumping power and reactor size is at a very high reactor pressure drop. At the Mach 2, 1800° F point the helium compressor power is 20 percent of the air compressor power. This illustrates the importance of shield weight even at small reactor diameters. The high power extraction lowers the specific impulse and increases the required total airflow to provide the specified thrust.

Comparison at 35,000-Foot Altitude

Without an attempt to estimate the temperature levels at which the systems will be operable, a performance comparison is made in figure 4. Arbitrary temperature ranges of 400° F spread are used to cover the areas of interest. All values are for an altitude of 35,000 feet and 500,000 pounds of gross weight.

The upper and lower bounds of the band for the direct-air system correspond to effective reactor wall temperatures of 2400° and 2000° F, respectively. These values are rather high, according to experimental results reported, but it is apparent that the direct-air system will require fuel-element temperatures of over 2200° F to show good payload capability at supersonic speeds. This conclusion should not, however, be construed to mean that the direct-air system is inferior for other design points.

The band for the lithium system has a spread of effective reactor wall temperature from 1900° to 1500° F. If bimetal heat exchangers of good efficiency can be developed to take advantage of the properties of columbium, performance in the upper part of the band is to be expected.

[redacted]

E-196

However, if stainless steel or nickel-base alloys must be used, the lower limit may even be too high. By comparison with the direct-air system, though, the lithium system shows impressive performance at any temperature and Mach number in the ranges shown.

The performance of the helium system is given for maximum heat-exchanger wall temperatures from 2000° to 1600° F. The helium-system temperature level is chosen lower than that for the direct-air system because of the extreme pressure stresses which the exchanger must withstand to contain the helium. The performance of the helium system is close enough to that of the lithium system to make them competitive, especially because of the uncertainty with regard to allowable temperature levels.

Other Effects

The effect of design altitude variation is shown in figure 5. Payload values for the three systems for the same temperature ranges as in figure 4 are plotted against altitude. Since gross weight and lift-drag ratio remain constant, thrust is constant. The principal effect is a change in the required total airflow and, thus, in the weight of air-handling equipment. In the direct-air system the reactor is included in the air-handling equipment, and the performance falls off rapidly as altitude is increased. The lithium and helium systems are less drastically affected.

The radiation dose rate at the crew compartment is another of the important parameters affecting nuclear aircraft performance. Figure 6 shows the variation of payload with dose rate for the three systems. The middle line of each band corresponds to the middle temperature of the previously defined temperature spreads. The widths of the bands correspond to ±20 percent variations in shield weight to account for the uncertainties in the shield-weight calculation procedure. All other calculations for this study were made for a dose rate of 0.5 rem/hr.

Both the small slopes and the narrow widths of the bands for the lithium and helium systems indicate that there is a relatively small penalty associated with either dose-rate variation or shield-weight inaccuracy where the reactor size is small. However, the direct-air-system calculations indicate that a change in dose rate or a 20-percent change in weight has a relatively large effect on payload capability.

An aircraft parameter subject to considerable uncertainty is the lift-drag ratio, and the effect of an arbitrary variation of L/D is shown in figure 7. All other calculations of this study use an L/D of 6.6 at Mach 2. Since the gross weight remains constant, the lift is

constant, and a change in L/D means a change in drag. To compensate, the amount of air-handling equipment must change. As in the altitude effect, the systems with low powerplant weights are least affected by L/D change, whereas the direct-air system is strongly affected.

System Characteristics

To illustrate the relative magnitudes of the component weights more clearly, table I shows weight breakdowns for the three systems. The same temperature spreads as used previously are shown except for the direct-air system which will not fly at Mach 2 with the low temperature.

The point made previously regarding the enormous shield weights in the direct-air system is clearly illustrated in table I. The reactors are about 7 to 8 feet in diameter, and the disadvantage of the air-cooled reactor with such high airflow requirements is obvious. Use of two reactors would make the reactor diameter more reasonable, but the total shield weight would be even higher than for the one large reactor. Note that because of the high shield weight the optimum compressor pressure ratios are 14.5 and 16 at the design point.

The next column in table I is for the lithium system at 1500° to 1900° F effective reactor wall temperatures. The low shield weights are due to the fact that the reactors are only 2.1 feet in diameter, assuming the power density is not excessive. The engine weights are also small because of the low compression ratio. The last column is for the helium system at 1600° to 2000° F maximum heat-exchanger wall temperatures. The reactors and shields weigh only slightly more than those for the lithium system because the reactor cores are 2.5 feet in diameter. For both the helium and lithium systems engine weights are small because the pressure ratio is at its minimum value, and the heat-exchanger weights are also relatively small. The payloads increase from the direct-air system to the helium system to the lithium system, with little difference between the latter two for the temperature ranges shown.

SUMMARY OF RESULTS

The results of the comparison of nuclear propulsion systems for logistic-type aircraft are summarized below. The payload values quoted are intended to be used primarily for relative comparison rather than as first estimates of expected performance.

1. For effective reactor wall temperatures between 1500° and 1900° F, the lithium system is estimated to give a 500,000-pound aircraft a

E-196

payload capability of about 200,000 to 220,000 pounds at flight Mach numbers from subsonic to above 2.5 at a 35,000-foot altitude.

2. For maximum heat-exchanger wall temperatures between 1600° and 2000° F, the helium system is estimated to give payloads of about 170,000 to 190,000 pounds under the same conditions.

3. For an effective reactor wall temperature of 2400° F, the direct-air system is estimated to give payloads of about 100,000 pounds at speeds up to Mach 2, but the payload values drop rapidly with temperatures below this level and at Mach numbers higher than 2. The direct-air system requires extremely large reactors for propulsion of such a large aircraft at supersonic speeds.

4. The lithium and helium systems, being characterized by small reactors, are less sensitive to changes in altitude, allowable dose rate, and aircraft lift-drag ratio than is the direct-air system.

Lewis Research Center
National Aeronautics and Space Administration
Cleveland, Ohio, December 23, 1958

E-196

[redacted]

APPENDIX A

SYMBOLS

A	flow area, sq ft
B	coefficient in optimization-procedure fitted equation
C_f	coefficient in heat-exchanger friction-factor correlation equation
C_h	coefficient in heat-exchanger heat-transfer correlation equation
C_v	velocity coefficient of nozzle
c_p	specific heat, Btu/(lb)($^\circ$F)
$\mathscr{D}_{50}$	dose rate at 50 ft from reactor center, rem/hr
d	diameter, ft
d_e	equivalent diameter, ft
F	thrust, lb
f	Fanning friction factor
G	mass velocity, lb/(sec)(sq ft)
g	gravitational acceleration, 32.17 ft/sec^2
H	enthalpy, Btu/lb
h	heat-transfer coefficient, Btu/(sq ft)(sec)($^\circ$F)
J	conversion factor from Btu to ft-lb
j	product of Stanton number and Prandtl number
k	thermal conductivity, Btu/(sec)(ft)($^\circ$F)
L/D	aircraft lift-drag ratio
l	length, ft
M	Mach number
N_E	number of engines per powerplant

[redacted]

E-196

N_L	number of lines between an engine and reactor
N_{Nu}	Nusselt number, hd_e/k
N_P	number of passes in heat exchanger
N_{Pe}	Peclet number, $Gd_e c_p/k$, or $N_{Re}N_{Pr}$
N_{Pr}	Prandtl number, $\mu c_p/k$
N_{Re}	Reynolds number, Gd_e/μ
N_{St}	Stanton number, $h/c_p G$, or $N_{Nu}/N_{Pr}N_{Re}$
P	total pressure, lb/sq ft
$\mathscr{P}$	compressor pressure ratio
p	static pressure, lb/sq ft
Q	power
R	gas constant, ft/^{o}F
S	surface area, sq ft
S/V	surface-area - volume ratio
T	total temperature, ^{o}R
t	static temperature, ^{o}R
th	thickness, ft
v	velocity, ft/sec
W	weight, lb
$\mathscr{W}$	ratio of turbine work to compressor work
w	weight-flow rate, lb/sec
x	value of independent variable in optimization-procedure fitted equation
α	free-flow ratio (flow area/frontal area)
γ	ratio of specific heats

[redacted]

δ dimensionless pressure ratio, P_0/p_{sl}

ϵ effectiveness of heat exchanger or reactor

η efficiency of compressor, turbine, pump, or fin

θ dimensionless temperature ratio, T_0/t_{sl}

μ viscosity, lb/(ft)(sec)

ρ density, lb/cu ft

Subscripts:

b bulk (average of inlet and outlet)

C compressor

E engine

EX heat exchanger

eff effective

F fin

f film (average of bulk and wall)

fr friction

GB gear box

g gross (weight)

He helium

ID inner diameter

L line

Li Lithium

lm log mean (temperature difference)

max maximum

mom momentum

E-196

[redacted]

N	normal (third dimension of heat exchanger, normal to two flow directions)
n	nozzle
OD	outer diameter
oa	over-all
P	pump
PL	payload
PP	powerplant
R	reactor
RS	reactor-shield assembly
ST	structure
sl	sea level
T	turbine
W	wall
0	free stream

E-196

E-196

APPENDIX B

ASSUMPTIONS AND METHODS OF CALCULATION

Common Assumptions

The assumptions and reference data used in the thermodynamic and weight analyses of the three propulsion systems consist of certain common items and others which are peculiar to the particular system. The common assumptions and data are listed in this section; the descriptions of those for the individual systems follow in separate sections.

Variations of ambient pressure, temperature, and speed of sound with altitude are in accordance with the ICAO standard atmosphere. Ratios of static to total temperature and pressure as functions of Mach number in the free stream are taken from reference 1.

Physical properties of air as found in reference 2 are used in order to be consistent with the empirical heat-exchanger performance correlations therein. Variations of specific heat at constant pressure, viscosity, and thermal conductivity with temperature are shown in figure 8, along with the approximate exponential relations used in the analyses to facilitate machine computations. The same property variations are used throughout all cycles except in the reactor of the direct-air system, which does not use a correlation from reference 2, as is explained in the next section. The ratio of specific heats is assumed to be 1.4 in the inlet, compressor, and heat-exchanger inlet and 1.34 in the heat-exchanger outlet, turbine, and nozzle. In the application of the heat-transfer correlation from reference 2, a constant value of Prandtl number equal to 0.65 is used.

In all heat-transfer processes, heat-transfer coefficients and friction pressure drops are calculated using the film-temperature method described in reference 3. To illustrate, the following equations are used to calculate h and Δp_{fr} when a heat exchanger from reference 2 is involved:

$$h = j c_{p,f} G_f N_{Pr}^{-2/3} \tag{B1}$$

where

$$j = N_{St,f} N_{Pr}^{2/3} = \frac{h}{c_{p,f} G_f} (0.65)^{2/3} = \Phi_f(N_{Re,f})$$

$$G_f = \rho_f v = \frac{w}{A} \frac{T_b}{T_f}$$

$$N_{Re,f} = \frac{G_f d_e}{\mu_f} = \frac{w d_e T_b}{A \mu_f T_f}$$

$$\Delta p_{fr} = f \frac{l}{d_e} \frac{G_f^2}{g} \left(\frac{1}{\rho_1} + \frac{1}{\rho_2} \right)_f \tag{B2}$$

where

$$f = \Phi_f(N_{Re,f})$$

$$\left(\frac{1}{\rho_1} + \frac{1}{\rho_2} \right)_f = \left(\frac{1}{\rho_1} + \frac{1}{\rho_2} \right)_b \frac{T_f}{T_b}$$

Note that the subscripts f and b refer to evaluation of a function at film and bulk temperature, respectively. Film temperature is defined as the arithmetic average of wall and bulk temperatures, and bulk temperature is the average of inlet and outlet fluid temperatures. In terms of c_p and μ evaluated at film temperature and ρ and G evaluated at bulk temperature, the equations may be written

$$h = \Phi_f(N_{Re,f})^{1.333} c_{p,f} G_b \frac{T_b}{T_f} \tag{B3}$$

and

$$\Delta p_{fr} = \Phi_f(N_{Re,f}) \frac{l}{d_e} \frac{G_b^2}{g} \frac{T_b}{T_f} \left(\frac{1}{\rho_1} + \frac{1}{\rho_2} \right)_b \tag{B4}$$

The turbojet engines for all systems are of the same family, compression ratio and airflow being variable. Both compressor and turbine are assigned polytropic efficiencies of 88 percent. A velocity coefficient of 97 percent is assumed for the fully expanding nozzle. The inlet-diffuser total-pressure ratio varies with flight Mach number as shown in figure 9. The subsonic portion of the curve assumes a loss in dynamic pressure of 0.08 q_0; the supersonic portion corresponds roughly to three-shock external-compression recovery with 5-percent internal loss.

Turbojet weight is computed as the sum of a compressor term and a turbine term with the reference weights based on an analysis of turbojet engines (ref. 4)

$$W_E = F_C W_{air} \frac{\sqrt{\theta_1}}{\delta_1} \ln \mathscr{P} + F_T W_{air} \frac{\sqrt{T_{T,1}}}{P_{T,1}} \ln \frac{P_{T,1}}{P_{T,2}} \tag{B5}$$

where $F_C = 5.0$ and $F_T = 1315.0$. Both compressor and turbine weights are shown to be proportional to corrected airflow and the logarithm of the pressure ratio. Engine weight being proportional to airflow, total engine weight is determined by total airflow rather than number and size of engines. No additional installation or casing weights are included; such weights are assumed to be accounted for in the F_C and F_T factors.

The aircraft are assumed to be unaffected by cycle type. All have a gross weight of 500,000 pounds, 30 percent of which is structure. The other 70 percent less reactor, shield, and powerplant is available for payload. The assumed variation of aircraft lift-drag ratio with flight Mach number is shown in figure 10 (unpublished data). The effect of L/D variation is estimated for each system because of the uncertainty of a parameter so much a function of aircraft configuration. A 20-percent thrust margin is reserved for maneuverability at all design points, so that the design altitudes are not absolute ceilings. No allowance is made for chemical fuel; any such weight will have to be taken out of the payload.

E-196

Direct-Air System

The reactors for the direct-air-cycle powerplants are optimized in diameter, length, and effectiveness. Free-flow-ratio and shield-weight determinations are described in appendix C.

With specified values of reactor diameter, length, and effectiveness and with estimated heat-transfer and pressure-drop characteristics, the required passage equivalent diameter can be determined. Corresponding values of heat-transfer coefficient and friction factor are calculated from

$$N_{Nu,f} = 0.028(N_{Re,f})^{0.8}(N_{Pr,f})^{0.4} \tag{B6}$$

and

$$f = 0.063(N_{Re,f})^{-0.2} \tag{B7}$$

These equations are adaptations of the empirical correlations from the stacked-plate tests of reference 5, the principal difference being a reduced coefficient in the friction-factor equation to account for the addition of more sections.

For consistency with the empirical correlations of reference 5, physical-property relations for air identical to those used in reduction of the test data are used in the reactor performance calculation. These

relations are shown as dotted lines in figure 8. Combining these exponential temperature functions with equations (B6) and (B7) gives

$$h = 0.00041 \frac{G_b^{0.8}}{d_e^{0.2}} \frac{T_b^{0.8}}{T_f^{0.728}} \tag{B8}$$

and

$$\Delta p_{fr} = \left[0.010534 (G_b d_e)^{-0.2} \frac{T_b^{0.8}}{T_f^{0.664}} \right] \frac{l_R}{d_e} \frac{G_b^2}{g} \left(\frac{1}{\rho_1} + \frac{1}{\rho_2} \right) \tag{B9}$$

E-196

Pressure and temperature drops in the ducting between the direct-air reactor and the turbojet engines are assumed to be 2 percent between compressor outlet and reactor inlet and 3 percent between reactor outlet and turbine inlet.

The fuel-element effective wall temperature is specified, but several values are used to show the effect of this very important parameter. No estimate is made of maximum wall temperature. Effective wall temperature is defined as that uniform temperature which gives the same overall heat-transfer performance as an actual, nonuniform temperature distribution.

A complete list of equations used in the analysis of the direct-air system is given on the following pages arranged for convenient computation on a digital computor. Many of these equations are common to the liquid-metal and helium systems, as is noted in the next two sections. The station numbering system is:

0	free stream, diffuser inlet
1	diffuser outlet, compressor inlet
2	compressor outlet
3	reactor inlet
4	reactor outlet
5	turbine inlet
6	turbine outlet, nozzle inlet
n	nozzle outlet

First, the compressor inlet temperature is calculated from

$$\theta_1 = \frac{t_0/t_{sl}}{t_0/T_0} \tag{B10}$$

$$T_1 = \theta_1 t_{sl} \tag{B11}$$

The compressor outlet temperature can be calculated from the known inlet conditions and the assumed efficiency

$$T_2 = (\mathscr{P})^{\frac{\gamma-1}{\gamma \eta_C}} T_1 \tag{B12}$$

The compressor enthalpy rise is calculated for later use

$$\Delta H_C = c_{p,C}(T_2 - T_1) \tag{B13}$$

where $c_{p,C}$ is based on $T_C = 0.5(T_2 + T_1)$. The compressor inlet pressure is the product of the stagnation pressure and the diffuser pressure ratio

$$\delta_0 = \frac{p_0/p_{sl}}{p_0/P_0} \tag{B14}$$

$$\delta_1 = \delta_0 \frac{P_1}{P_0} \tag{B15}$$

$$P_1 = \delta_1 p_{sl} \tag{B16}$$

Compressor outlet pressure

$$P_2 = (\mathscr{P})P_1 \tag{B17}$$

can then be calculated. Since the pressure and temperature losses in the compressor-to-reactor ducting are assumed to be known, the reactor inlet conditions can be calculated from the expressions

$$P_3 = (P_3/P_2)P_2 \tag{B18}$$

$$T_3 = (T_3/T_2)T_2 \tag{B19}$$

The reactor flow area

$$A_3 = \frac{\pi}{4} d_R^2 \alpha_R \tag{B20}$$

E-196

can be determined (see appendix C for α_R), and the reactor mass velocity

$$G_3 = \frac{W_{air,total}}{A_3} \tag{B21}$$

can be calculated from an assumed total airflow. The Mach number follows using an equation from compressible-flow theory

$$M_3 = G_3 \frac{\sqrt{T_3}}{P_3} \sqrt{\frac{R}{\gamma g}} \left(1 + \frac{\gamma - 1}{2} M_3^2\right)^{\frac{\gamma+1}{2(\gamma-1)}} \tag{B22}$$

E-196

Static temperature and pressure at the reactor inlet

$$t_3 = T_3\left(1 + \frac{\gamma - 1}{2} M_3^2\right)^{-1} \tag{B23}$$

$$p_3 = P_3(t_3/T_3)^{\frac{\gamma}{\gamma-1}} \tag{B24}$$

can be calculated and used to determine inlet density

$$\rho_3 = \frac{p_3}{Rt_3} \tag{B25}$$

With the reactor effectiveness specified, the outlet temperature can be found from

$$T_4 = \epsilon_R(T_{W,R} - T_3) + T_3 \tag{B26}$$

The analysis requires knowledge of bulk and film temperatures

$$T_b = 0.5(T_3 + T_4) \tag{B27}$$

$$T_f = 0.5(T_b + T_{W,R}) \tag{B28}$$

The log-mean-temperature difference follows

$$\Delta T_{lm} = \frac{T_4 - T_3}{\ln\left(\frac{T_{W,R} - T_3}{T_{W,R} - T_4}\right)} \tag{B29}$$

The reactor heat-transfer surface area

$$S_R = 4 \frac{A_3 l_R}{d_e} \tag{B30}$$

may be computed from known geometry. The required heat-transfer coefficient

$$h = \frac{w_{air,total} c_{p,b} (T_4 - T_3)}{S_R \Delta T_{lm}} \tag{B31}$$

may be compared with the attainable coefficient to determine the required fuel-element equivalent diameter

$$h = 0.00041 \frac{G_3^{0.8}}{d_e^{0.2}} \frac{T_b^{0.8}}{T_f^{0.728}} \tag{B32}$$

With this value of d_e the pressure drop may be calculated from the equations

$$\Delta p_{fr} = \left[0.010534 (G_3 d_e)^{-0.2} \frac{T_b^{0.8}}{T_f^{0.664}} \right] \frac{l_R}{d_e} \frac{G_3^2}{g} \left(\frac{1}{\rho_3} + \frac{1}{\rho_4} \right) \tag{B33}$$

$$\Delta p_{mom} = \frac{G_3^2}{g \rho_3} \left(\frac{\rho_3}{\rho_4} - 1 \right) \tag{B34}$$

The reactor outlet conditions follow

$$p_4 = p_3 - \Delta p_{fr} - \Delta p_{mom} \tag{B35}$$

$$G_3 \frac{\sqrt{T_4}}{p_4} \sqrt{\frac{R}{\gamma g}} = M_4 \left(1 + \frac{\gamma - 1}{2} M_4^2 \right)^{1/2} \tag{B36}$$

$$t_4 = T_4 \left(1 + \frac{\gamma - 1}{2} M_4^2 \right)^{-1} \tag{B37}$$

$$\rho_4 = \frac{p_4}{R t_4} \tag{B38}$$

$$P_4 = p_4 \left(\frac{T_4}{t_4} \right)^{\frac{\gamma}{\gamma - 1}} \tag{B39}$$

E-196

Turbine inlet conditions

$$P_5 = P_4\left(\frac{P_5}{P_4}\right) \tag{B40}$$

$$T_5 = T_4\left(\frac{T_5}{T_4}\right) \tag{B41}$$

can now be determined using the duct performance. Since turbine work equals compressor work, the turbine outlet conditions can be calculated from

$$T_6 = T_5 - \frac{\Delta H_C}{c_{p,T}} \tag{B42}$$

where $c_{p,T}$ is based on $T_T = \frac{T_5 + T_6}{2}$, and

$$P_6 = P_5\left(\frac{T_6}{T_5}\right)^{(\gamma-1)\eta_T} \tag{B43}$$

Nozzle performance can then be determined from the equations

$$t_n = T_6\left(\frac{p_0}{P_6}\right)^{\frac{\gamma-1}{\gamma}} \tag{B44}$$

$$\Delta H_n = c_{p,n}(T_6 - t_n) \tag{B45}$$

where $c_{p,n}$ is based on $T_n = \frac{T_6 + t_n}{2}$. Using the jet velocity

$$v_j = \sqrt{C_v^2 2gJ\ \Delta H_n} \tag{B46}$$

and the flight velocity

$$v_0 = M_0 a_0 \tag{B47}$$

the specific impulse

$$\frac{F}{w_{air}} = \frac{v_j - v_0}{g} \tag{B48}$$

[redacted]

and the total thrust

$$F_{total} = 1.2 \frac{W_g}{(L/D)} \tag{B49}$$

can be calculated. Also the airflow

$$w_{air} = \frac{F_{total}}{(F/w_{air})} \tag{B50}$$

can be calculated and compared with the previously assumed value. After all iterations are complete, the engine weights

$$W_E = 5 \frac{w_{air}}{N_E} \frac{\sqrt{\theta_1}}{\delta_1} \ln \mathscr{P} + 1315 \frac{w_{air}}{N_E} \frac{\sqrt{T_5}}{P_5} \ln\left(\frac{P_5}{P_6}\right) \tag{B51}$$

can be combined into powerplant weight

$$W_{PP} = W_E N_E \tag{B52}$$

By subtracting powerplant, reactor-shield-assembly, and structure weights from gross weight, the payload

$$W_{PL} = \left(1 - \frac{W_{ST}}{W_g}\right) W_g - W_{PP} - W_{RS} \tag{B53}$$

can be determined. The reactor-shield-assembly weight is determined as explained in appendix C.

Liquid-Metal System

The liquid-metal-to-air heat exchanger in the lithium powerplant is one of the finned flat-tube configurations of reference 2. The geometry was not optimized in the sense that over-all aircraft performance was computed for several exchanger core types, but the type chosen (from fig. 105, p. 119, of ref. 2) is representative of high-performance, compact-core heat exchangers suitable for this application. A sketch of the surface, a list of pertinent characteristics, the correlation curves, and the analytical approximations used in the machine calculations are shown in figure 11. Two lithium passes inside the tubes are assumed, so that no cross-flow correction factor is included in the analysis.

The air-side fins are assumed to be of stainless-steel-clad copper having a thermal conductivity of 108 Btu/(hr)(ft)($^{\circ}$F) and a density of

[redacted]

E-196

524 pounds per cubic foot. The tubes are assumed to be of stainless steel or some other material of comparable density (491 lb/cu ft) with 0.016-inch-thick walls. Headers are estimated to be tube continuations between passes and line-to-exchanger transitions at the inlet and outlet. Heat-exchanger sections of about 4-square-foot frontal area are assumed to be encased in tube material of 0.125-inch thickness. Material of the same gage is assigned for the inlet and outlet headers. The resulting heat-exchanger density, including a 15-percent increase for brazing or welding material, is about 76.5 pounds per cubic foot.

In contrast to the direct-air-system analysis, no change in temperature or pressure is introduced between compressor outlet and heat-exchanger inlet or between exchanger outlet and turbine inlet.

The physical properties of lithium at temperatures up to about 2000° R are fairly well known with the exception of thermal conductivity, for which data are unavailable above 1500° R, and it seems unreasonable to extrapolate from the lower temperature points. Variations of viscosity and thermal conductivity with temperature are shown in figure 12 along with some experimental measurements and the approximate exponential relations used in the analysis. Specific heat was assumed to be constant at 1.0 Btu/(lb)($^{\circ}$F) and density constant at 30.0 pounds per cubic foot.

The heat-transfer coefficient for a liquid metal flowing in a smooth passage is computed from a correlation found in reference 6

$$N_{Nu} = 0.625\, N_{Pe}^{0.4} = 0.625(N_{Re}N_{Pr})^{0.4} \tag{B54}$$

A friction-factor correlation identical to that for air in a smooth tube (ref. 4)

$$f = 0.046\, N_{Re}^{-0.2} \tag{B55}$$

was used in the computation of lithium pressure drops. Substituting the approximate exponential relations for the physical properties of lithium into the equations for h and ΔP gives

$$h_{Li} = 0.15\, \frac{G_{Li}^{0.4}}{d_{e,Li}^{0.6}}\, T_{Li}^{-0.24} \tag{B56}$$

and

$$\Delta P_{Li} = \left[0.0347\, \frac{T_{Li}^{-0.1913}}{(G_{Li}d_{e,Li})^{0.2}}\right] 2\, \frac{l_{Li}}{d_{e,Li}}\, \frac{G_{Li}^2}{g\rho_{Li}} \tag{B57}$$

All lithium properties are evaluated at bulk temperature because the differences between bulk and film temperatures will be very small.

Both reactor flow area and lithium line diameter are functions of maximum permissible lithium velocity. From considerations of corrosion and design experience, velocities of 40 and 10 feet per second were chosen for the reactor and lines, respectively.

The lithium lines are assumed to be of the same material as the heat-exchanger tubes (density, 519 lb/cu ft) with 0.24-inch-thick walls. The lines are assumed to be 10 feet long and to number two per engine. In calculating line pressure drop, 40 diameters are added to the length to account for bend and header losses. The weight of the metal lines plus lithium is increased 25 percent to account for insulation and structure.

The lithium is considered to be circulated by a pump which weighs 4 pounds per brake horsepower. The pump is assumed to be driven by the turbojet shaft through a gear box which weighs 0.1 pound per brake horsepower. The choice of this pump-drive system is not the result of an optimization study, but it affords simplicity of analysis and a representative weight. The gear-box weight is included to express the difference between systems rather than as an estimate of actual gearing weight, which would have a minimum practical value.

The maximum lithium temperature and the effective reactor fuel-element temperature are specified, being corrosion limited in accordance with the state of the art. The effect of variations in lithium temperature is shown because of the uncertainty of the corrosion limit.

A complete list of equations used in the analysis of the liquid-metal system follows. Where an equation is identical except for subscript notation to one listed in the direct-air-system section, only the equation number is listed. The station numbering system is:

0 free stream, diffuser inlet (air)

1 diffuser outlet, compressor inlet (air)

2 compressor outlet, heat-exchanger inlet (air)

3 heat-exchanger outlet, turbine inlet (air)

4 turbine outlet, nozzle inlet (air)

n nozzle outlet (air)

5 heat-exchanger inlet (lithium)

E-196

6 heat-exchanger outlet, pump inlet (lithium)

7 pump outlet (lithium)

8 reactor inlet (lithium)

9 reactor outlet (lithium)

E-196

Equations (B10) and (B17) can be used to compute compressor inlet and outlet conditions and heat-exchanger inlet conditions. With the specified value of heat-exchanger inlet Mach number the mass velocity

$$G_2 = \frac{p_2}{\sqrt{T_2}} \sqrt{\frac{\gamma g}{R_{air}}}\, M_2 \left(1 + \frac{\gamma - 1}{2} M_2^2\right)^{-\frac{\gamma+1}{2(\gamma-1)}} \tag{B58}$$

can be calculated. Equations (B23) to (B25) with the subscript 2 give other exchanger inlet conditions. From the specified fluid temperatures and maximum wall temperature, the average wall temperature

$$T_{W,EX} = T_{b,air} + \frac{T_{EX,max} - T_3}{T_5 - T_3} (T_{b,Li} - T_{b,air}) \tag{B59}$$

can be determined, where $T_{b,air} = 0.5(T_2 + T_3)$ and $T_{b,Li} = 0.5(T_5 + T_6)$. The Reynolds number follows

$$N_{Re,f,air} = \frac{G_2 d_{e,air}}{\mu_{f,air}} \frac{T_{b,air}}{T_{f,air}} \tag{B60}$$

where

$$T_{f,air} = 0.5(T_{W,EX} + T_{b,air})$$

The heat-transfer coefficient can be calculated from the fitted correlation curves by the relation

$$h_{air} = 1.333\, c_{p,f,air} G_2 \frac{T_{b,air}}{T_{f,air}} \left(C_{h,1} + C_{h,2} N_{Re,f,air}^{C_{h,3}}\right) \tag{B61}$$

The fin efficiency is calculated from an approximate equation found in standard heat-transfer texts

$$\eta_F = \frac{\tanh y}{y} \tag{B62}$$

[redacted]

where $y = l_F \sqrt{\frac{2h_{air}}{k_F th_F}}$. From the exchanger geometry the ratio of effective to total surface area is

$$\frac{S_{eff}}{S_{total}} = 1 - (1 - \eta_F) \frac{S_F}{S_{total}} \tag{B63}$$

Using the over-all log-mean-temperature difference

$$\Delta T_{lm,oa} = \frac{(T_6 - T_2) - (T_5 - T_3)}{\ln\left(\frac{T_6 - T_2}{T_5 - T_3}\right)} \tag{B64}$$

the air-side length

$$l_{air} = \frac{G_2 c_{p,b,air}(T_3 - T_2)\alpha_{air}}{h_{air}\left(\frac{T_{W,EX} - T_{b,air}}{T_{b,Li} - T_{b,air}}\right)\Delta T_{lm,oa} \frac{S_{eff}}{S_{total}} \left(\frac{S}{V}\right)_{air}} \tag{B65}$$

and the lithium-side length

$$l_{Li} = \left[\frac{\alpha_{air} G_2 c_{p,b,air}(T_3 - T_2)}{\alpha_{Li} c_{p,Li}(T_5 - T_6) l_{air}} d_{e,Li}\right]^{1.5} \left[\frac{\alpha_{Li} c_{p,Li}(T_5 - T_6) T_{b,Li}^{0.24}}{\left(\frac{S}{V}\right)_{Li} 0.15\, \Delta T_{lm,oa}\left(1 - \frac{T_{W,EX} - T_{b,air}}{T_{b,Li} - T_{b,air}}\right)}\right]^{2.5} \tag{B66}$$

may be determined. Lithium-side mass velocity and flow area follow

$$G_5 = \frac{\alpha_{air} G_2 c_{p,b,air}(T_3 - T_2)}{\alpha_{Li} c_{p,Li}(T_5 - T_6) l_{air}} l_{Li} \tag{B67}$$

$$A_5 = \frac{w_{Li}}{N_E G_5} \tag{B68}$$

The friction-pressure-drop equation

$$\Delta p_{fr,air} = \frac{l_{air}}{d_{e,air}} \frac{G_2^2}{g} \left(\frac{1}{\rho_2} + \frac{1}{\rho_3}\right)\left(C_{f,1} + C_{f,2} N_{Re,f,air}^{C_{f,3}}\right) \tag{B69}$$

[redacted]

E-196

and equations (B34) to (B39), with subscripts 2 and 3, may be solved for the exchanger outlet conditions. Lithium-side pressure drop is calculated using equation (B57) in the form

$$P_5 - P_6 = 0.0694 \frac{l_{Li}}{d_{e,Li}^{1.2}} \frac{G_5^{1.8}}{g\rho_{Li}} T^{-0.1913} \tag{B70}$$

E-196

The specified value of lithium velocity in the reactor is used to calculate mass velocity

$$G_8 = \rho_{Li} v_{Li,R} \tag{B71}$$

An assumed value of lithium flow rate is used to compute reactor flow area

$$A_8 = \frac{w_{Li}}{G_8} \tag{B72}$$

The allowable free-flow ratio, a function of diameter, may be combined with the flow area to determine the core diameter

$$d_R = \sqrt{\frac{4}{\pi} \frac{A_8}{\alpha_R}} \tag{B73}$$

(see appendix C for α_R). Since all reactor temperatures are specified, the log-mean-temperature difference can be calculated by use of

$$\Delta T_{lm,R} = \frac{T_5 - T_6}{\ln\left(\frac{T_{w,R} - T_6}{T_{w,R} - T_5}\right)} \tag{B74}$$

Then the attainable heat-transfer coefficient

$$h_R = 0.15 \frac{G_8^{0.4}}{d_{e,R}^{0.6}} T_{b,Li}^{-0.24} \tag{B75}$$

where $T_{b,Li} = 0.5(T_5 + T_6)$, and the required heat-transfer coefficient

$$h_R = \frac{G_8 c_{p,Li} (T_5 - T_6) d_{e,R}}{4 l_R \Delta T_{lm,R}} \tag{B76}$$

can be equated to solve for the fuel-element equivalent diameter $d_{e,R}$. The specified lithium velocity in the lines determines the line diameter

$$d_L = \sqrt{\frac{w_{Li}}{N_E(N_L/2)(\pi/4)\rho_{Li}v_{Li,L}}} \tag{B77}$$

The reactor pressure drop may be computed from

$$P_8 - P_9 = 0.0694 \frac{l_R}{d_{e,R}^{1.2}} \frac{G_8^{1.8}}{g\rho_{Li}} T_{b,R}^{-0.1913} \tag{B78}$$

Using an effective line length

$$l_{eff} = l_L + \left(\frac{l}{D}\right)_L d_L \tag{B79}$$

to account for bend losses, the line pressure drops can be calculated as

$$P_7 - P_8 = 0.0694 \frac{l_{eff}}{d_L^{1.2}} \frac{\rho_{Li}^{0.8} v_{Li,L}^{1.8}}{g} T_6^{-0.1913} \tag{B80}$$

$$P_9 - P_5 = 0.0694 \frac{l_{eff}}{d_L^{1.2}} \frac{\rho_{Li}^{0.8} v_{Li,L}^{1.8}}{g} T_5^{-0.1913} \tag{B81}$$

The total-pressure drop determines the pump power and the ratio of turbine to compressor work

$$\mathscr{W} = 1 + \frac{c_{p,b,air}(T_3 - T_2)\left[(P_5 - P_6) + (P_7 - P_8) + (P_8 - P_9) + (P_9 - P_5)\right]}{778.2\, c_{p,Li}(T_5 - T_6)\Delta H_C \rho_{Li} \eta_P} \tag{B82}$$

Then, the air turbine exit conditions, nozzle performance, thrust, and airflow follow from

$$T_4 = T_3 - \frac{\mathscr{W}\Delta H_C}{c_{p,T}} \tag{B83}$$

where $c_{p,T}$ is based on $T_T = 0.5(T_3 + T_4)$ and equations (B43) to (B50) with subscripts 3 and 4. From the airflow rate the lithium flow rate can

be calculated and compared with the assumed value. The iteration procedure converges rapidly by using the new value of w_{Li} in equation (B72) and repeating the process

$$w_{Li} = \frac{c_{p,b,air}(T_3 - T_2)}{c_{p,Li}(T_5 - T_6)} w_{air} \tag{B84}$$

The dimension of the heat exchanger normal to air-side and lithium-side lengths is given by

$$l_N = \frac{w_{air} N_P}{N_E G_2 \alpha_{air} l_{Li}} \tag{B85}$$

Total air-side flow area follows

$$A_2 = \frac{w_{air}}{N_E G_2} \tag{B86}$$

The exchanger weight can be calculated from dimensions and densities

$$W_x = \frac{l_{air} l_{Li} l_N}{N_P} (\rho_x + \alpha_{Li} \rho_{Li}) \tag{B87}$$

Line weights can also be computed

$$W_L = 1.25\, \pi d_L th_L l_L N_L \rho_L + \frac{\pi}{4} d_L l_L N_L \rho_{Li} \tag{B88}$$

The pump power

$$Q_P = 1.417(\mathscr{W} - 1) \frac{w_{air}}{N_E} \Delta H_C \tag{B89}$$

results in an estimate of pump weight

$$W_P = 4Q_P \tag{B90}$$

The variable portion of the gear-box weight

$$W_{GB} = 0.1\, Q_P \tag{B91}$$

is calculated from the horsepower also. Equation (B51) gives the engine weight, which may be combined with the other component weights to give total powerplant weight

$$W_{PP} = N_E(W_E + W_{EX} + W_L + W_P + W_{GB}) \tag{B92}$$

E-196

Equation (B53) then gives payload, with W_{RS} determined as in appendix C.

Helium System

The helium system is very nearly identical to the liquid-metal system. Besides the change in heat-transfer fluid, the only major differences are in the helium lines and pumps. The helium-to-air heat exchanger is assumed to be of the same geometry as its counterpart in the liquid-metal system, but the structural material is molybdenum with a density of 637 pounds per cubic foot instead of a material weighing 491 pounds per cubic foot. The resulting heat-exchanger density is 96.3 pounds per cubic foot, and the effective thermal conductivity of the molybdenum-and-copper fins is 133 Btu/(hr)(ft)(^{o}F).

E-196

The physical properties of helium, as given in reference 7, are plotted in figure 13. Also shown are the approximate exponential relations used in the computing-machine analysis. The specific heat at constant pressure is 1.25, and the ratio of specific heats is 1.667.

Heat-transfer and friction-factor correlations for helium are assumed to be identical to those for air in smooth passages, as found in reference 3. In nondimensional form the correlations are

$$N_{Nu,f} = 0.0216(N_{Re,f})^{0.8}(N_{Pr,f})^{0.4} \tag{B93}$$

and

$$f = 0.046(N_{Re,f})^{-0.2} \tag{B94}$$

When the exponential temperature functions for μ and k and the constant value of c_p are combined, the equations for h and Δp_{fr} become

$$h = 0.00157 \frac{G_b^{0.8} T_b^{0.8}}{d_e^{0.2} T_f^{0.6688}} \tag{B95}$$

and

$$\Delta p_{fr} = \left[0.002162(G_b d_e)^{-0.2} \frac{T_b^{0.8}}{T_f^{0.6706}}\right] \frac{l}{d_e} \frac{G_b^2}{g} \left(\frac{1}{\rho_1} + \frac{1}{\rho_2}\right) \tag{B96}$$

The helium line weights are based on a double-wall model. An inner duct of molybdenum withstands the high temperature. A gap of 1/2 inch

filled with high-pressure stagnant helium and insulation separates the inner and outer ducts. The outer duct, made of Inconel at 519 pounds per cubic foot, withstands the high pressure while at a temperature of not more than 1000° F. The inner duct is assumed to be 0.030 inch thick, whereas the outer-duct thickness is determined from stress considerations. The allowable stress in the outer duct is assumed to be 80,000 psi. As in the liquid-metal system, the basic line weight is increased by 25 percent to account for structure, insulation, and so forth.

E-196

The diameter of the inner duct is determined by helium flow rate, density, and specified pressure drop. Without detailed layouts of the powerplants, the best pressure drop cannot be determined, but a value of 1/2 percent in each line is used.

The helium compressor is assumed to have a polytropic efficiency of 85 percent, and its weight is calculated using a relation similar to that for air-compressor weight

$$W_P = \frac{w_{He}}{N_E} \sqrt{T_6} \ln\left(\frac{P_7}{P_6}\right) \tag{B97}$$

The omission of the pressure from the denominator makes the pump weight proportional to helium pressure.

A complete list of equations used in the analysis of the helium system is given on the following pages. Where duplication of an equation listed previously in the appendix would serve no useful purpose, the equation number is listed instead. The station numbering system is identical to that in the liquid-metal system.

Equations (B10) to (B17), (B58), (B23) to (B25) with the subscript 2, and (B59) to (B65) are used to compute inlet, compressor, and heat-exchanger conditions. The helium-side length

$$l_{He} = \left[\frac{\alpha_{air} G_2 c_{p,b,air}(T_3 - T_2)}{\alpha_{He} c_{p,He}(T_5 - T_6) l_{air}} d_{e,He}\right]^{0.25} \left[\frac{\alpha_{He} c_{p,He}(T_5 - T_6) T_{f,He}^{0.6688}}{\left(\frac{S}{V}\right)_{He} 0.00157\, \Delta T_{lm,oa} T_{b,He}^{0.8} \left(1 - \frac{T_{W,EX} - T_{b,air}}{T_{b,He} - T_{b,air}}\right)}\right]^{1.25} \tag{B98}$$

follows from equation (B95) and an expression like equation (B31). Equations (B67) to (B69) with the subscript He instead of Li and (B34) to (B39) with subscripts 2 and 3 give helium-side area and air-side outlet conditions by means of an iterative solution. The helium outlet Mach number is calculated from the equation

$$G_5 \frac{\sqrt{T_6}}{P_6} \sqrt{\frac{R_{He}}{\gamma g}} = M_6 \left(1 + \frac{\gamma - 1}{2} M_6^2\right)^{-\frac{\gamma+1}{2(\gamma-1)}} \tag{B99}$$

[redacted]

Also, the other helium conditions at the heat-exchanger outlet can be calculated from

$$t_6 = T_6\left(1 + \frac{\gamma - 1}{2} M_6^2\right)^{-1} \tag{B100}$$

$$p_6 = P_6\left(1 + \frac{\gamma - 1}{2} M_6^2\right)^{-\frac{\gamma}{\gamma-1}} \tag{B101}$$

$$\rho_6 = \frac{p_6}{R_{He} t_6} \tag{B102}$$

Helium inlet conditions can be determined by solving the following four equations simultaneously:

$$p_5 = p_6 + \frac{G_5^2}{g\rho_6}\left(1 - \frac{\rho_6}{\rho_5}\right) + 0.002162 \frac{l_{He} G_5^{1.8} T_{b,He}^{0.8}}{d_{e,He}^{1.2} g T_{f,He}^{0.6706}}\left(\frac{1}{\rho_5} + \frac{1}{\rho_6}\right) \tag{B103}$$

$$\rho_5 = \frac{p_5}{R_{He} t_5} \tag{B104}$$

$$t_5 = T_5\left(1 + \frac{\gamma - 1}{2} M_5^2\right)^{-1} \tag{B105}$$

$$G_5 \frac{\sqrt{T_5}}{p_5}\sqrt{\frac{R_{He}}{\gamma g}} = M_5\left(1 + \frac{\gamma - 1}{2} M_5^2\right)^{1/2} \tag{B106}$$

Reactor outlet total pressure can be calculated using the specified line pressure ratio

$$P_9 = P_5\left(\frac{P_9}{P_5}\right) \tag{B107}$$

With α_R again calculated from equation (C1), the reactor flow area and mass velocity are

$$A_8 = \frac{\pi}{4} d_R^2 \alpha_R \tag{B108}$$

$$G_8 = \frac{w_{He}}{A_8} \tag{B109}$$

E-196

The value of helium weight flow is assumed to start the iteration for gross weight. The outlet Mach number and static parameters follow

$$G_8 \frac{\sqrt{T_5}}{P_9} \sqrt{\frac{R_{He}}{\gamma g}} = M_9 \left(1 + \frac{\gamma - 1}{2} M_9^2\right)^{-\frac{\gamma+1}{2(\gamma-1)}} \tag{B110}$$

$$t_9 = T_9 \left(1 + \frac{\gamma - 1}{2} M_9^2\right)^{-1} \tag{B111}$$

$$p_9 = P_9 \left(1 + \frac{\gamma - 1}{2} M_9^2\right)^{-\frac{\gamma}{\gamma-1}} \tag{B112}$$

$$\rho_9 = \frac{p_9}{R_{He} t_9} \tag{B113}$$

On the inlet side of the reactor the total pressure can be related to the pump outlet pressure by

$$P_8 = P_7 \left(\frac{P_8}{P_7}\right) \tag{B114}$$

The reactor inlet total temperature is the exchanger outlet temperature multiplied by the temperature ratio of the pump

$$\frac{T_8}{T_6} = \left(\frac{P_7}{P_6}\right)^{\frac{\gamma-1}{\gamma \eta_P}} \tag{B115}$$

For the machine calculations a value of T_8 was assumed at this point. The inlet Mach number follows

$$G_8 \frac{\sqrt{T_8}}{P_8} \sqrt{\frac{R_{He}}{\gamma g}} = M_8 \left(1 + \frac{\gamma - 1}{2} M_8^2\right)^{-\frac{\gamma+1}{2(\gamma-1)}} \tag{B116}$$

also the inlet static parameters

$$t_8 = T_8 \left(1 + \frac{\gamma - 1}{2} M_8^2\right)^{-1} \tag{B117}$$

[redacted]

$$p_8 = P_8\left(1 + \frac{\gamma - 1}{2} M^2\right)^{-\frac{\gamma}{\gamma-1}} \tag{B118}$$

$$\rho_8 = \frac{p_8}{R_{He} t_8} \tag{B119}$$

The friction pressure drop

$$\Delta p_{fr,R} = p_8 - p_9 - \frac{G_8^2}{g\rho_9}\left(1 - \frac{\rho_9}{\rho_8}\right) \tag{B120}$$

and the log-mean-temperature difference in the reactor

$$\Delta T_{lm,R} = \frac{T_5 - T_8}{\ln\left(\frac{T_{W,R} - T_8}{T_{W,R} - T_5}\right)} \tag{B121}$$

can be computed. A solution for the equivalent diameter

$$d_{e,R} = \left[0.002162 \frac{l_R G_8^{1.8} T_{b,R}^{0.8}}{\Delta p_{fr,R} g T_{f,R}^{0.6706}}\left(\frac{1}{\rho_8} + \frac{1}{\rho_9}\right)\right]^{1/1.2} \tag{B122}$$

and the attainable heat-transfer coefficient follow

$$h_R = 0.00157 \frac{G_8^{0.8} T_{b,R}^{0.8}}{d_{e,R}^{0.2} T_{f,R}^{0.6688}} \tag{B123}$$

By use of these quantities, attainable and required reactor power can be equated to determine the accuracy of the T_8 estimation

$$Q_R = h_R \, 4 \frac{l_R A_8}{d_{e,R}} \Delta T_{lm,R} \tag{B124}$$

$$Q_R = w_{He} c_{p,He}(T_5 - T_8) \tag{B125}$$

After the iteration for T_8 is complete, the pumping power is determined from

$$\Delta H_P = c_{p,He}(T_8 - T_6) \tag{B126}$$

[redacted]

$$\mathscr{W} = 1 + \frac{\Delta H_p w_{He}}{\Delta H_c w_{air}} \qquad \text{(B127)}$$

Equations (B83), (B43) to (B50) with subscripts 3 and 4, and (B84) to (B87) with the subscript He instead of Li complete the performance calculation, including the iteration for w_{He}, and the calculation of exchanger weight. Equation (B79) gives effective line length. The average pressure drop per line

$$\Delta P_L = 0.5\left[(P_9 - P_5) + (P_7 - P_8)\right] \qquad \text{(B128)}$$

and the mass velocity in the lines

$$G_L = \frac{2w_{He}}{N_E N_L \frac{\pi}{4} d_2^2} \qquad \text{(B129)}$$

can be combined to give

$$\Delta P_L = 0.002162 \frac{l_{eff} G_L^{1.8} T_{b,R}^{0.1294}}{d_L^{1.2} g}\left(\frac{1}{\rho_8} + \frac{1}{\rho_9}\right) \qquad \text{(B130)}$$

which is used to calculate the line diameter by trial-and-error. The thickness of the outer duct is determined by pressure and allowable stress

$$th_{OD} = \frac{P_7(d_L + 0.0833)}{2.304 \times 10^7} \qquad \text{(B131)}$$

The line weight follows

$$W_L = 1.25\, \pi l_L N_L\left[d_{ID} th_{ID} \rho_{ID} + (d_{ID} + 0.0833) th_{OD} \rho_{OD}\right] \qquad \text{(B132)}$$

The pump power

$$Q_P = 1.417\, \Delta H_P \frac{w_{He}}{N_E} \qquad \text{(B133)}$$

is then used with equation (B97) to give pump weight. Equations (B91), (B51), (B92), and (B53) are then used to compute other weights and the payload.

E-196

[redacted]

APPENDIX C

REACTOR AND SHIELD DATA

Reactor Diameter and Free-Flow-Ratio Data

The reactors for the three nuclear systems are all members of the family illustrated in figure 14. A beryllium oxide moderator and 6-inch-thick beryllium reflectors are assumed. Molybdenum for fuel elements and structure is included by assuming molybdenum volume equal to 15 percent of void volume. The moderator-to-uranium atom ratio is 400. The presence of a particular coolant was neglected. Criticality calculations were made using the method of reference 14.

The curves of figure 14 are approximated for machine computation by the following equations:

Reactor $l/d = 1$, $d_R \leq 3$ feet

$$\alpha_R = \frac{2.363 - (d_R - 3.22)^2}{4.61} \tag{C1}$$

Reactor length variable, $3 \leq d_R \leq 9$, $2.5 \leq l_R \leq 4$

$$(\alpha_R - C)^2 - (d_R - B)^2 + E(\alpha_R - C)(d_R - B) = A \tag{C2a}$$

where

$$A = \frac{655.2}{4.807 - l_R} - 91.31 \tag{C2b}$$

$$B = 0.3282\ l_R - 1.1235 \tag{C2c}$$

$$C = 0.0857\ l_R + 0.42505 \tag{C2d}$$

$$E = 664.15 - \frac{2626.9}{5.2282 - l_R} \tag{C2e}$$

Reactor-Shield-Assembly Weight Data

The shield-weight calculations were made using the simplified model shown in figure 15. The crosshatched areas represent materials within the shield: reactor core, reflector, and pressure shell. The unshaded areas in the reactor are coolant headers, which are treated as voids in the generalized analysis. Around the pressure shell are located the

[redacted]

gamma and neutron shields, divided into three sections for the analysis. The location of the point at which the allowable dose rate is specified is 50 feet away on the reactor-shield-assembly centerline. A dose rate of 0.5 rem/hr was used for the basic comparison only.

As described in the previous section, the reactor core is composed of beryllium oxide, molybdenum, and uranium; the reflector is 6-inch-thick beryllium. The pressure shell is 4 inches of columbium and is all around. The headers are assumed to be 6 inches thick. The shield materials are depleted uranium for the gamma shield and lithium hydride for the neutron shield. The same materials and dimensions are used for all systems, with diameter, length, and power being the only variables. The thickness of the pressure shell is arbitrary. No stress calculations or cooling calculations were made. Thermal shields would have to be included in an actual design, but for this preliminary study the metal was all lumped into one piece.

E-196

The dose rate calculations used the following data sources and techniques:

(1) Nuclear cross sections from reference 8

(2) Gamma scattering data from reference 9

(3) Neutron scattering probabilities in accordance with reference 10, with the simplification of assumed isentropic scattering

(4) Buildup factor approximated by the number of relaxation lengths

(5) Neutron source strength (leakage) taken to be 1 percent of the fission source on the basis of a comparison with shield-weight calculations made in much greater detail (refs. 11 and 12)

(6) Gamma source strength taken to be five 3-mev gammas per fission

(7) Cylindrical reactor core reduced to a point source which gives specified source strength at core boundary

An approximation to optimum shield weight and shaping was obtained by (1) specifying that all solid angles of reactor-shield assembly contribute the same incremental dose rate at the crew compartment, and (2) varying the ratio of gamma dose to neutron dose from each section to give minimum shield-section weight. The principle of "equal doses from equal angles" is shown to be a good approximation to shield optimization in reference 8.

The resulting values of reactor-shield-assembly weight are plotted against reactor core diameter and power-dose ratio in figure 16. For

core diameters of 3 feet or less, a core length-diameter ratio of 1 is assumed. For the longer diameters length was allowed to vary to give optimum heat-transfer and pressure-drop characteristics. The effect of a change in length on reactor-shield-assembly weight is estimated to be equivalent to a simple extension or contraction of the basic assembly. The equations used in the machine computations to approximate the shield-weight family of curves are:

$l_R/d_R = 1$

$$W_{RS} = -35{,}000 - 40{,}000\, d_R + (17.5 + 33.4\, d_R)\left(\ln \frac{Q_R}{\mathscr{D}_{50}} + 40.4\right)^2 \quad (C3)$$

$l_R = 3$ feet

$$W_{RS,3} = 834{,}000 - 1500.1(d_R + 20.831)^2 + \left[148.3 + 3.685(d_R - 9.33)^2\right]\left[\ln \frac{Q_R}{\mathscr{D}_{50}} + 9.3\, d_R - 14.3\right]^2 \quad (C4)$$

l_R arbitrary

$$W_{RS} = W_{RS,3} + \frac{\pi}{4}(l_R - 3)\left[(1 - \alpha_R)d_R^2(181) + (2d_R + 1)(115) + \left(d_R + \frac{4}{3}\right)(739) + \left(d_R + \frac{14}{3}\right)(2400)\right] \quad (C5)$$

Q_R is in megawatts and $\mathscr{D}_{50}$ is in rem/hr.

To justify the use of this simplified weight estimation procedure, it is compared with two studies which treat similar shielding problems in some detail. A unit shield for an air-cooled reactor is reported in reference 11, and a unit shield for a helium-cooled reactor is reported in reference 12.

The direct-air-cycle reactor-shield assembly from reference 11 is designed for a 15,000-foot altitude, a core diameter and length of 2.5 feet, and a reactor-power - dose ratio of 26.4 megaw/(rem)(hr). The estimated weight is 66,000 pounds. From figure 16 and equation (C3), the reactor-shield-assembly weight for a 35,000-foot design point is 57,000 pounds. The difference is almost exactly the estimated difference due to altitude.

E-196

The helium-cycle reactor-shield assembly from reference 12 is designed for a 60,000-foot altitude, a core diameter and length of 3.3 feet, and a reactor-power - dose ratio of 1440 megaw/(rem)(hr). The estimated weight is 127,000 pounds. From equations (C4) and (C5), the reactor-shield-assembly weight for a 35,000-foot design point is 127,000 pounds. The effect of the design altitude difference is estimated to be about 25,000 pounds, which makes the simplified-analysis result of this study about 16 percent lighter. Of the difference, 10,000 pounds is due to a discrepancy between the fitted equation and the actual calculations. This inaccuracy is tolerated because the equations fit more accurately in the larger diameter range where they were used. The other 15,000 pounds is mostly due to a difference in reactor-core-weight estimation, but a 10-percent deviation is well within the actual accuracy of any unit shield calculation.

E-196

[redacted]

APPENDIX D

OPTIMIZATION PROCEDURE

The object of the optimization procedure is to determine the maximum payload capability of each of the three nuclear propulsion systems for specified values of flight Mach number, altitude, and other quantities which define the system state-of-the-art. Each aircraft-powerplant combination may be represented by an equation of the form

$$W_{PL} = \Phi(M_O, \text{Altitude}, \ldots, \mathscr{P}, T_3, \ldots) \qquad (D1)$$

The independent variables may be grouped into two categories: (1) design-point and state-of-the-art variables, and (2) optimization variables. In the first category, besides flight Mach number and altitude, are such quantities as the critical temperature in the system, the aircraft lift-drag ratio, and the allowable crew-compartment dose rate. Optimization variables, however, are those for which a best value can be determined for each combination of design-point and state-of-the-art variables. Included are such parameters as compressor pressure ratio, turbine inlet temperature, and reactor diameter.

The relations in the form of equation (D1) which define the three systems are complex and implicit, as shown in appendix B. Consequently, many values of the optimization parameter payload must be calculated for as many combinations of optimization variables in order that an approximate equation may be fitted in the form

$$W_{PL} = B_O + B_1 x_1 t \ldots + B_n x_n + B_{11} x_1^2 + \ldots$$
$$B_{nn} x_n^2 + B_{12} x_1 x_2 + \ldots + B_{n-3} x_{n-1} x_n \qquad (D2)$$

where n is the number of optimization variables. The maximum value of the optimization parameter as defined by the fitted equation may then be determined, if a maximum exists, along with the combination of optimization variables to which it corresponds.

Because of the many optimization variables, design points, and other variations to be investigated and because of the expense and scarcity of IBM 653 computing time, reduction of the total number of runs for the fitting of the general equations is very important. The incentive is similar to that for reduction of industrial experiments, such as in pilot plant operation, and of biological experiments. From these other fields of science have come methods of synthetic experiment design and optimization, as described in reference 13.

[redacted]

The saving in number of runs is shown in table II. The three-level factorial or "brute force" method would require a minimum of 3^n runs to determine the optimum point. The method of synthetic experiment design results in a run reduction for numbers of variables greater than two, with the improvement increasing rapidly as the number of variables increases. Reference 14 describes the utilization of this reduction in the field of reactor design.

E-196

Besides the reduction in number of runs, the other obvious advantage of the optimization procedure is elimination of curve plotting and lengthy interpretive periods between runs. Although at the probable expense of a loss in insight, the automatic optimization technique eliminates much of the tedious mechanics of the cycle analysis and thereby allows the investigator time to analyze the results.

The optimization variables for the three systems are listed in table III. Optimization was not always possible; for example, at high Mach number the liquid-metal system compressor pressure ratio $\mathscr{P}$ would have optimized at a value less than that required for takeoff. In this case a minimum $\mathscr{P}$ was specified, and $\mathscr{P}$ was eliminated from the optimization variables at the particular design point.

The optimization procedure used in this study has been coded for the IBM 653 computor in a form which will handle seven independent variables. Further information regarding the code can be obtained from the authors.

Actually, it should be noted that even the optimization just described required more computor time than was readily available because the particular systems being analyzed cannot be approximated satisfactorily with a general quadratic equation. Higher degree terms are necessary. Consequently, the optimization procedure was used to approach the true optimum. Fortunately, extreme accuracy was not required because of the nature of the study.

REFERENCES

1. Ames Research Staff: Equations, Tables, and Charts for Compressible Flow. NACA Rep. 1135, 1953. (Supersedes NACA TN 1428.)

2. Kays, W. M., and London, A. L.: Compact Heat Exchangers, The National Press, Palo Alto (Calif.), 1955.

3. Humble, Leroy V., Lowdermilk, Warren H., and Desmon, Leland G.: Measurements of Average Heat-Transfer and Friction Coefficients for the Subsonic Flow of Air in Smooth Tubes at High Surface and Fluid Temperatures. NACA Rep. 1020, 1951. (Supersedes NACA RM's E7L31, E8L03, E50E23, and E50H23.)

4. Manson, S. V., and Wachtl, William M.: A Design and Performance Study of the Nuclear Direct-Air-Cycle Supersonic Airplane, Including the Effects of Operating Temperature and Fuel Plate Material and Thickness. NACA RM E53C18, 1953.

5. Sams, Eldon W., and Weiland, Walter F., Jr.: Experimental Heat-Transfer and Friction Coefficient for Air Flowing Through Stacks of Parallel Flat Plates. NACA RM E54F11, 1954.

6. Lubarsky, Bernard, and Kaufman, Samuel J.: Review of Experimental Investigations of Liquid-Metal Heat Transfer. NACA Rep. 1270, 1956. (Supersedes NACA TN 3336.)

7. Akin, S. W.: Thermal Conductivity and Viscosity of Helium. Rep. 55141, Suppl., General Electric Co., July 1947.

8. Anon.: System 125A, Convair Model 25, Design Proposal. Shield Design Methods. Rep. FZA-25-075, Convair, Aug. 15, 1956.

9. Seale, R. L., and Humphries, C. E.: Air Scattered Gamma Dose Per Unit Source Strength for Various Shadow Shield Angles and Crew Shield Configurations. Rep. CVAC-244T, Convair, Apr. 9, 1954.

10. Stevenson, R.: Introduction to Nuclear Engineering. McGraw-Hill Book Co., Inc., 1954, p. 199.

11. Schmill, W. C., and Fogg, R. G.: Potentialities of Nuclear-Powered Turboprop. ANPD Report XDC-57-7-59, General Electric, July 1957.

12. Anon.: A Study of a Nuclear Propulsion System with Manned Supersonic Flight Potential. Rep. PWAC-202, (An Evaluation Study of Project RAND Report RM-1897), Pratt & Whitney Aircraft, Oct. 8, 1957.

13. Davies, Owen L.: The Design and Analysis of Industrial Experiments. Hafner Pub. Co., 1954.

14. Krase, J. M., and Cyl-Champlin, C.: Synthetic Experiment Design Technique in Reactor Analysis. Rep. APEX-303, General Electric, Nov. 30, 1956.

15. Webber, Henry A., Goldstein, David, and Fellinger, Robert C.: Determination of the Thermal Conductivity of Molten Lithium. Trans. ASME, vol. 77, no. 2, Feb. 1955, pp. 97-101; discussion, pp. 101-102.

E-196

16. Anon.: Liquid-Metals Handbook. NAVEXOS P-733, AEC and Bur. Ships, Navy Dept., June 1, 1950.

17. Novikov, I. I., et al.: The Heat-Transfer and High-Temperature Properties of Liquid Alkali Metals. Jour. Nuclear Energy, vol. 4, no. 3, Mar. 1957, pp. 387-408.

[redacted]

TABLE I. - WEIGHT BREAKDOWNS

[Mach number, 2.0; altitude, 35,000 ft; gross weight, 500,000 lb.]

	System		
	Direct-air	Lithium	Helium
Effective reactor wall temperature, °F	2200 to 2400	1500 to 1900	----------
Maximum heat-exchanger wall temperature, °F	----------	----------	1600 to 2000
Compressor pressure ratio	14.5 to 16	2.0	2.0
Reactor diameter, ft	7.7 to 6.8	2.1	2.5
Weight, thousands of lb			
Turbojet engines	43 to 36	24 to 16	25 to 18
Heat exchanger		41 to 21	51 to 30
Coolant circulation system		7	12 to 13
Reactor and shield	255 to 213	81	95 to 94
Total powerplant	298 to 249	153 to 125	183 to 155
Payload	52 to 101	197 to 225	167 to 195

E-196

[redacted]

E-196

TABLE II. - COMPARISON OF SYNTHETIC AND THREE-LEVEL FACTORIAL DESIGNS

Number of independent variables, n	Number of experimental points required	
	Synthetic design	Three-level factorial design
2	9	9
3	15	27
4	25	81
5	43	243
6	77	729
7	143	2187

[redacted]

TABLE III. - OPTIMIZATION VARIABLES

System		
Direct-air	Liquid-metal	Helium
$\mathscr{P}$	$\mathscr{P}$	$\mathscr{P}$
d_R	T_3	T_3
l_R	$T_{EX,max}$	T_5
R	T_6	T_6
	M_2	M_2
		P_6
		d_R

E-196

[redacted]

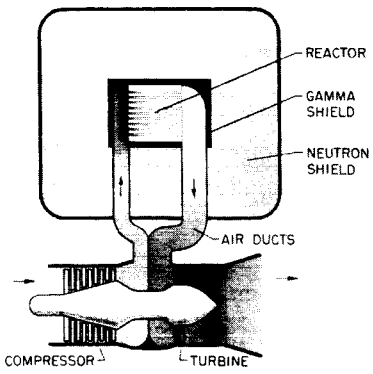

CS-14776

Disadvantages

Poor fluid
Large reactor, heavy shield
Fuel-element oxidation

Advantages

Simplicity
No intermediate temperature change
No pumping work

CS-14773

(a) Direct-air system.

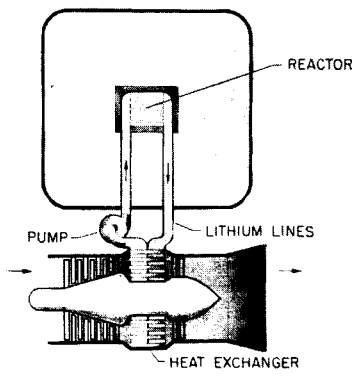

CS-14774

Disadvantages

Isotope separation
Corrosion, mass transfer
Heat-exchanger material selection problem
Pumping work

Advantages

No intermediate heat exchanger
Good fluid
Small reactor, light shield

CS-14771

(b) Lithium system.

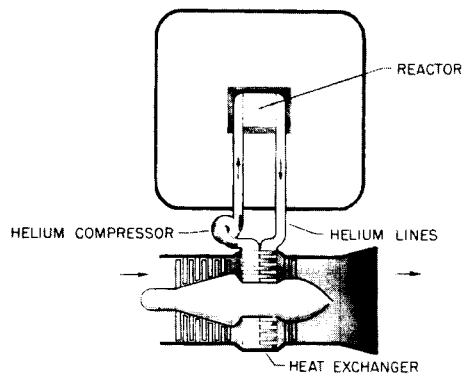

CS-14775

Disadvantages

High pressure
Heat-exchanger oxidation
Pumping work

Advantages

Small reactor, light shield
Inert gas
No intermediate heat exchanger

CS-14772

(c) Helium system.

Figure 1. - Schematic diagrams of propulsion systems.

E-196

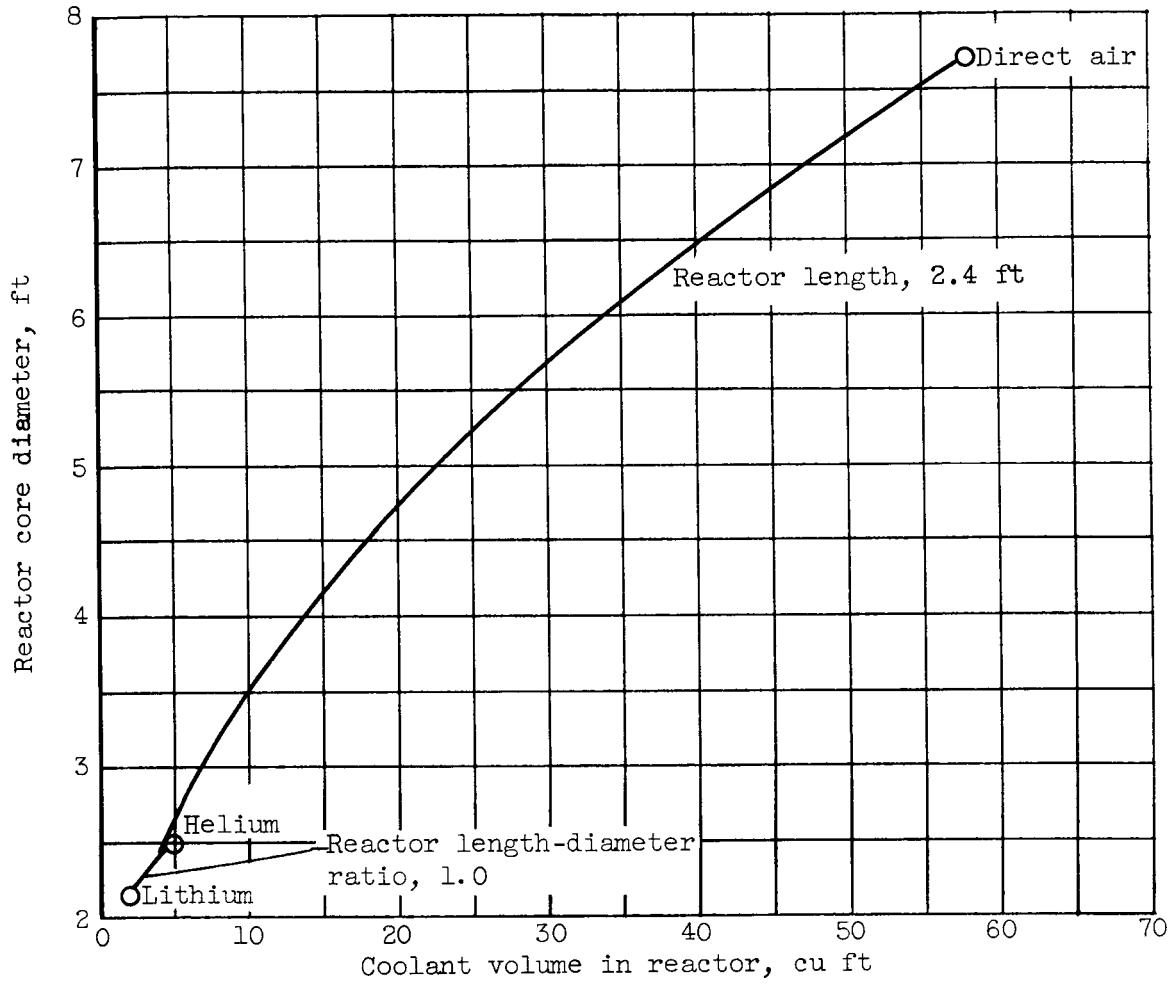

Figure 2. - Relative performance of reactor coolants. Power being removed from reactor, approximately 800 megawatts.

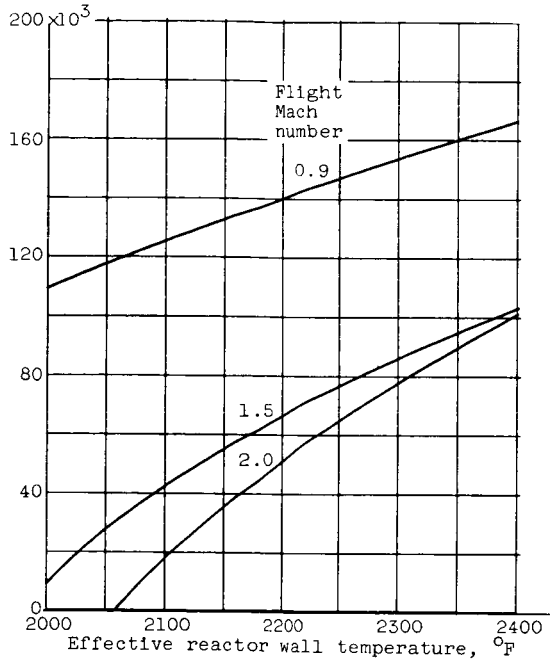

(a) Direct-air system.

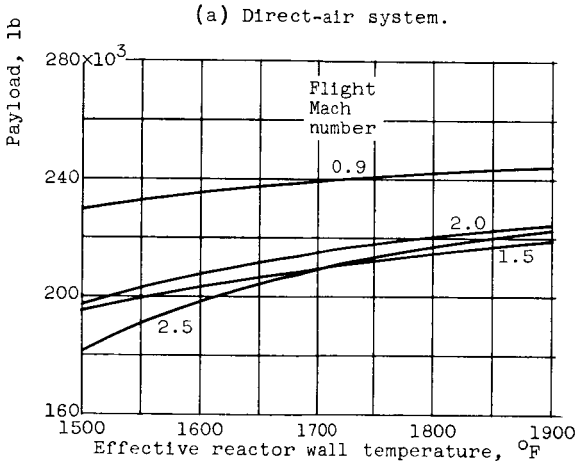

(b) Lithium system.

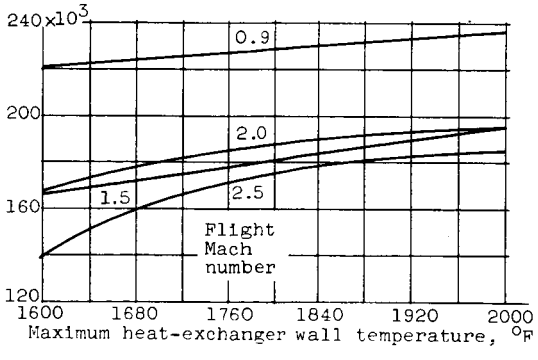

(c) Helium system.

Figure 3. - Variation of payload with operating temperature.

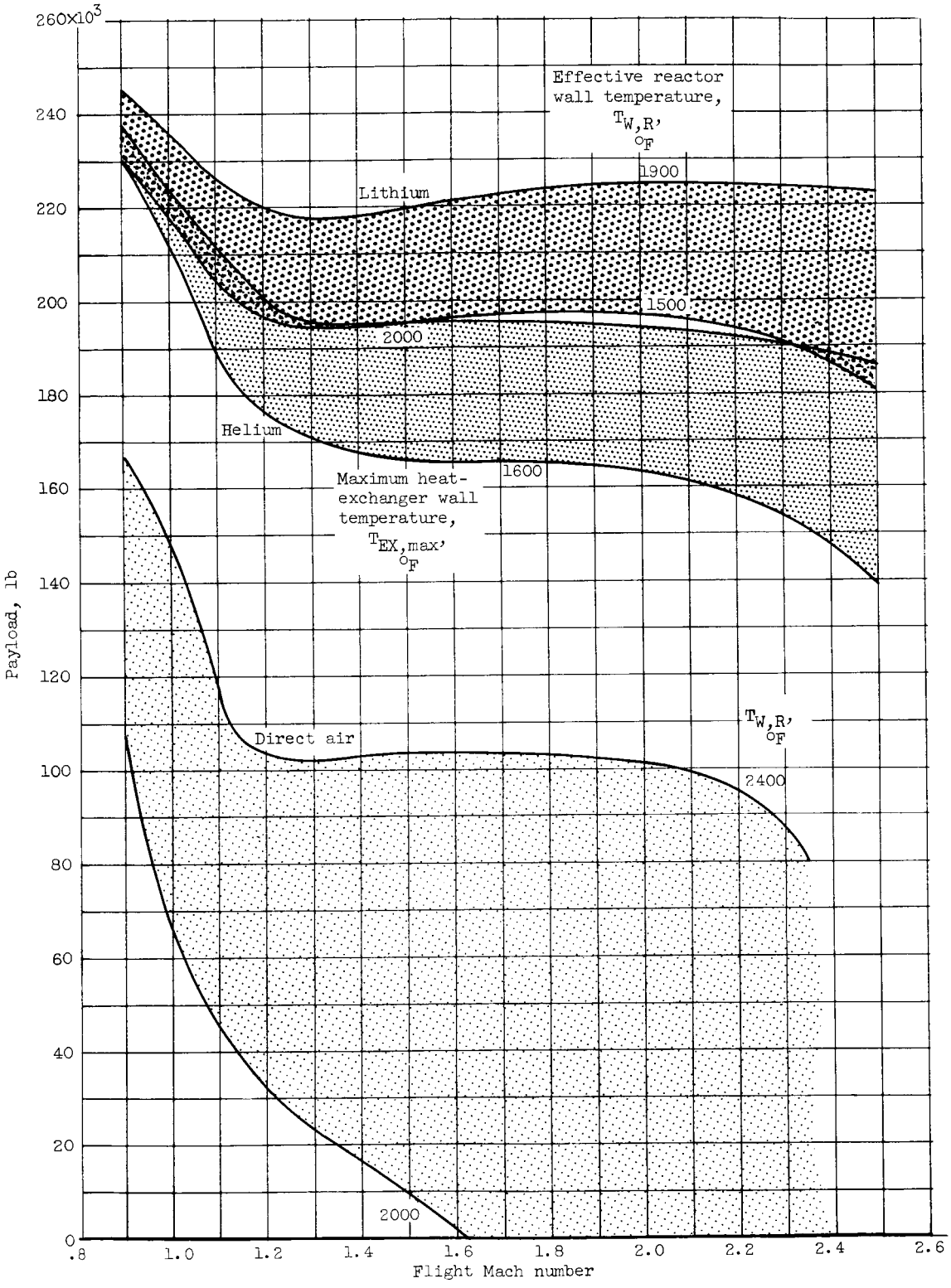

Figure 4. - Payload plotted against flight Mach number. Gross weight, 500,000 pounds; altitude, 35,000 feet.

CONFIDENTIAL

E-196

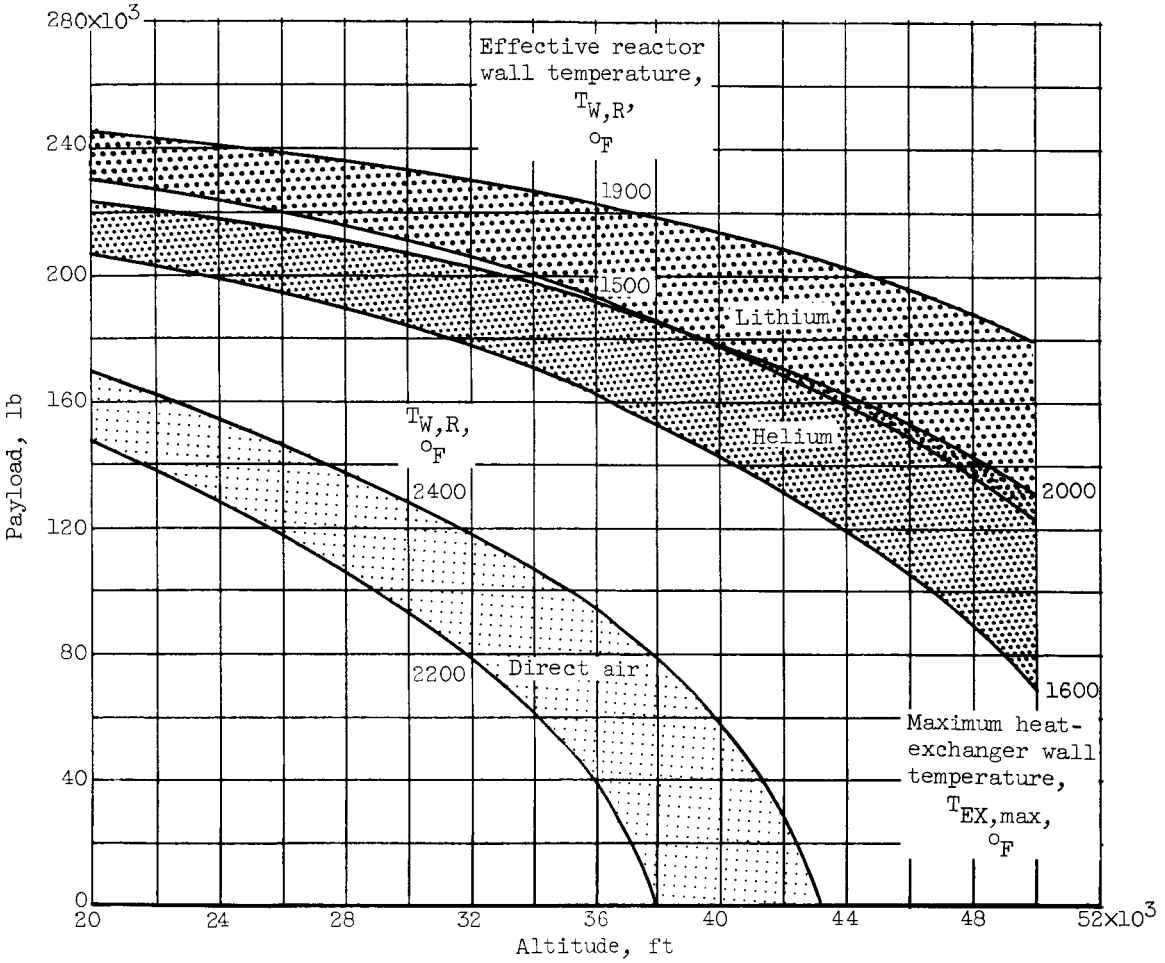

Figure 5. - Effect of variation in altitude. Flight Mach number, 2.0; gross weight, 500,000 pounds.

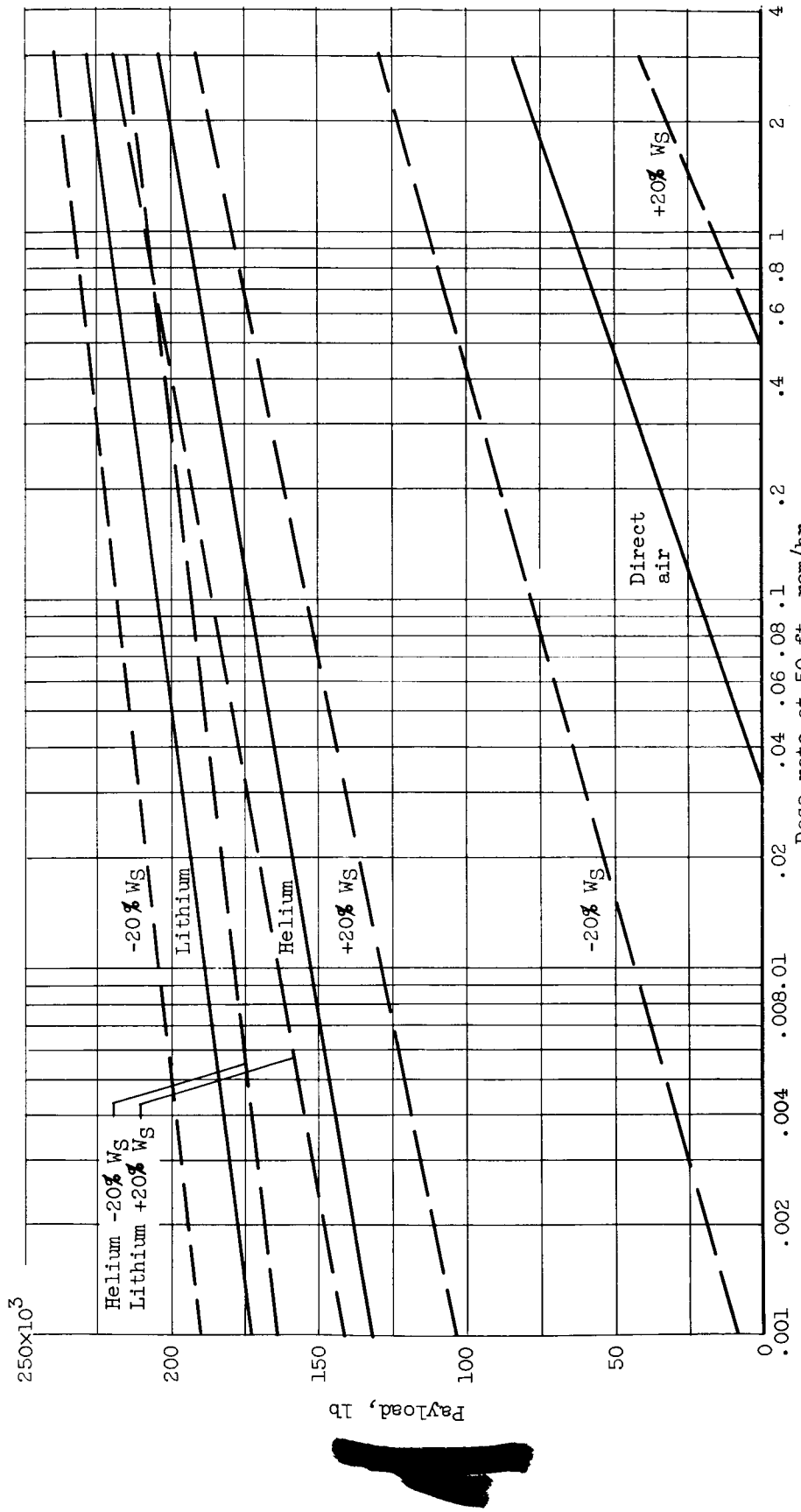

Figure 6. - Effect of dose rate. Flight Mach number, 2.0; gross weight, 500,000 pounds. (W_S, shield weight.)

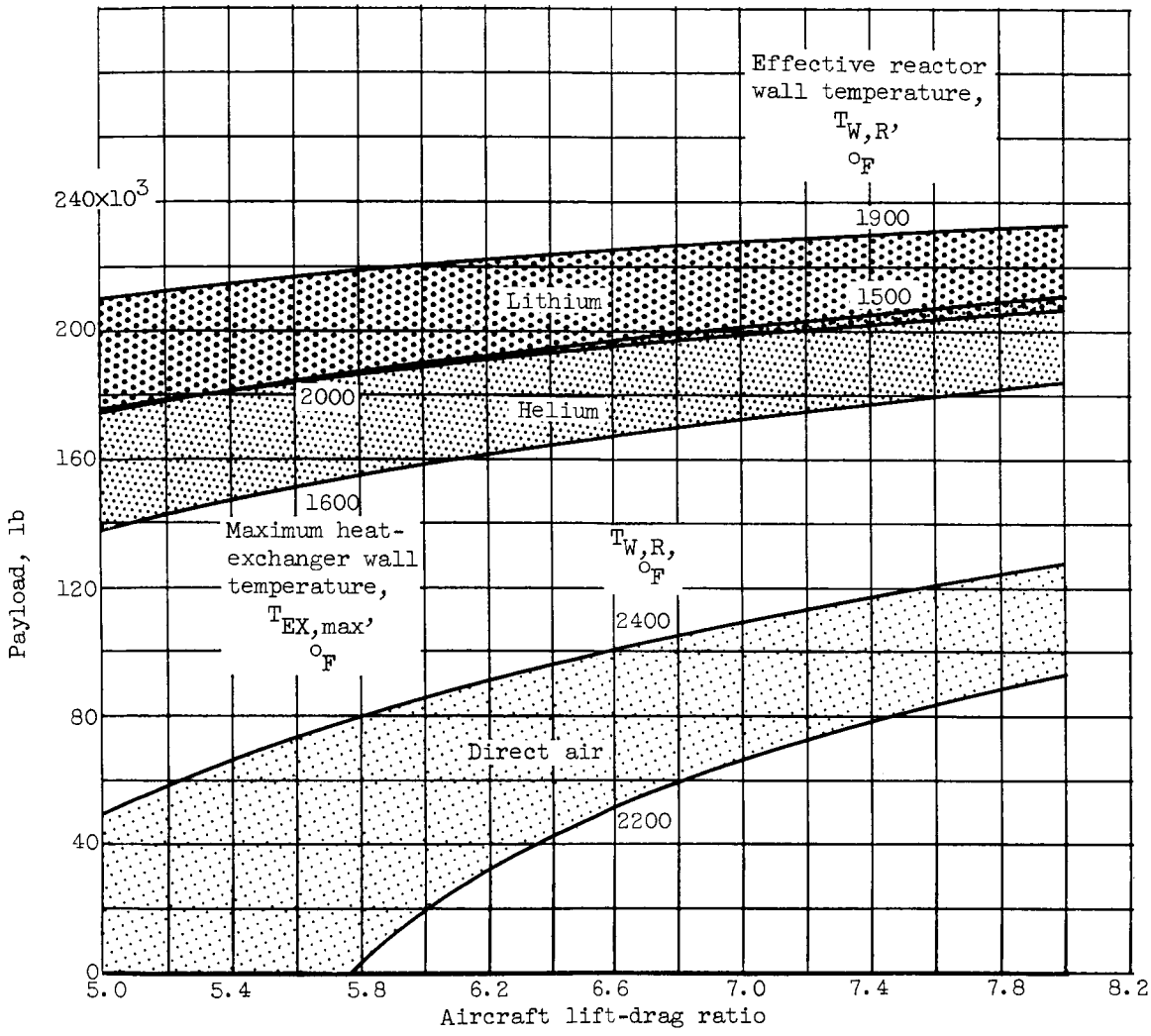

Figure 7. - Effect of variation in aircraft lift-drag ratio. Flight Mach number, 2.0; altitude, 35,000 feet; gross weight, 500,000 pounds.

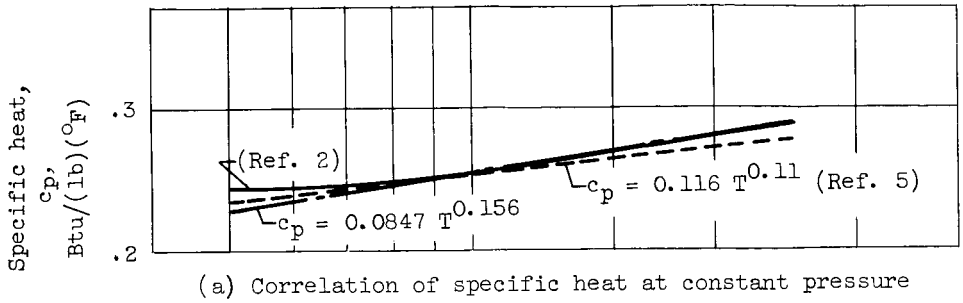

(a) Correlation of specific heat at constant pressure with temperature.

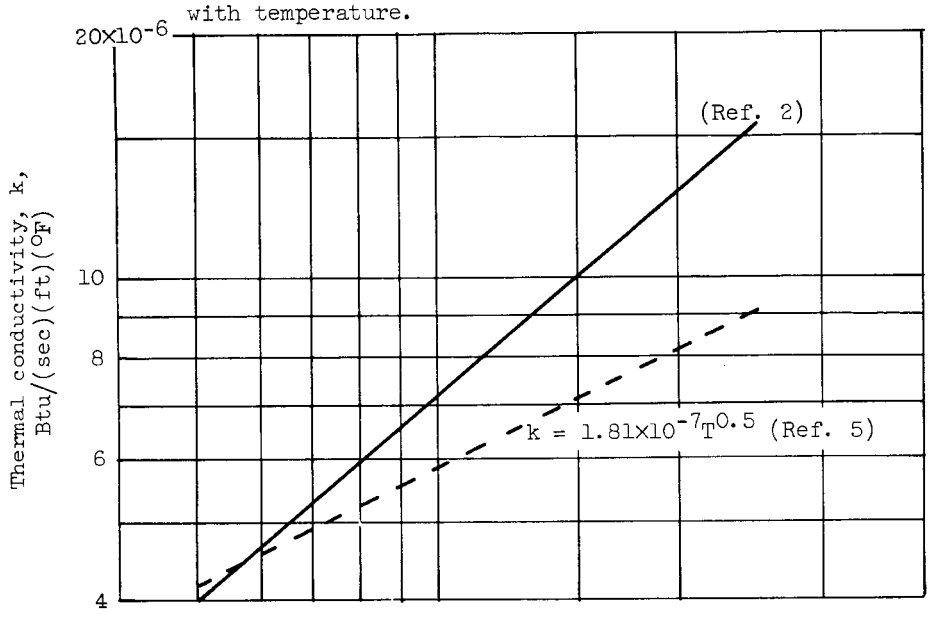

(b) Correlation of thermal conductivity with temperature.

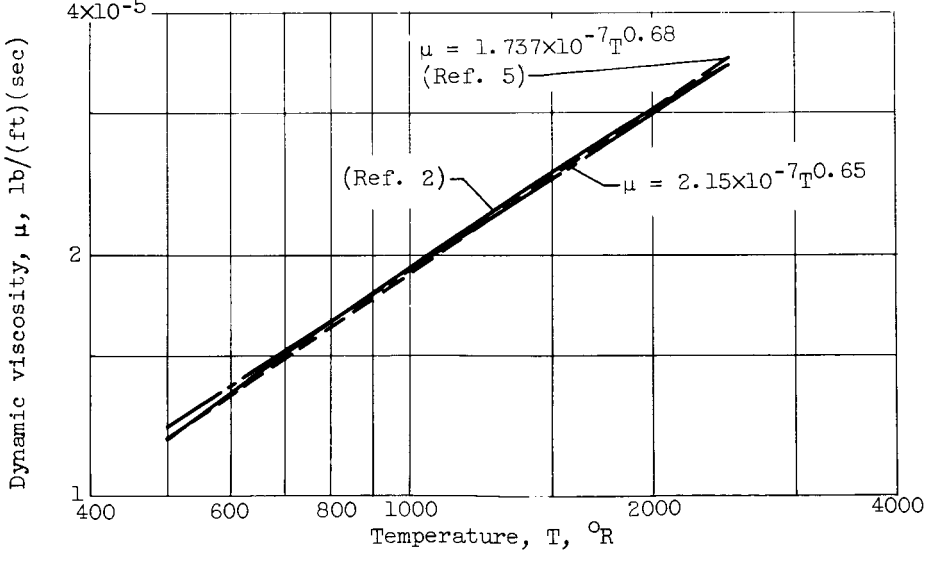

(c) Correlation of dynamic viscosity with temperature.

Figure 8. - Physical properties of air.

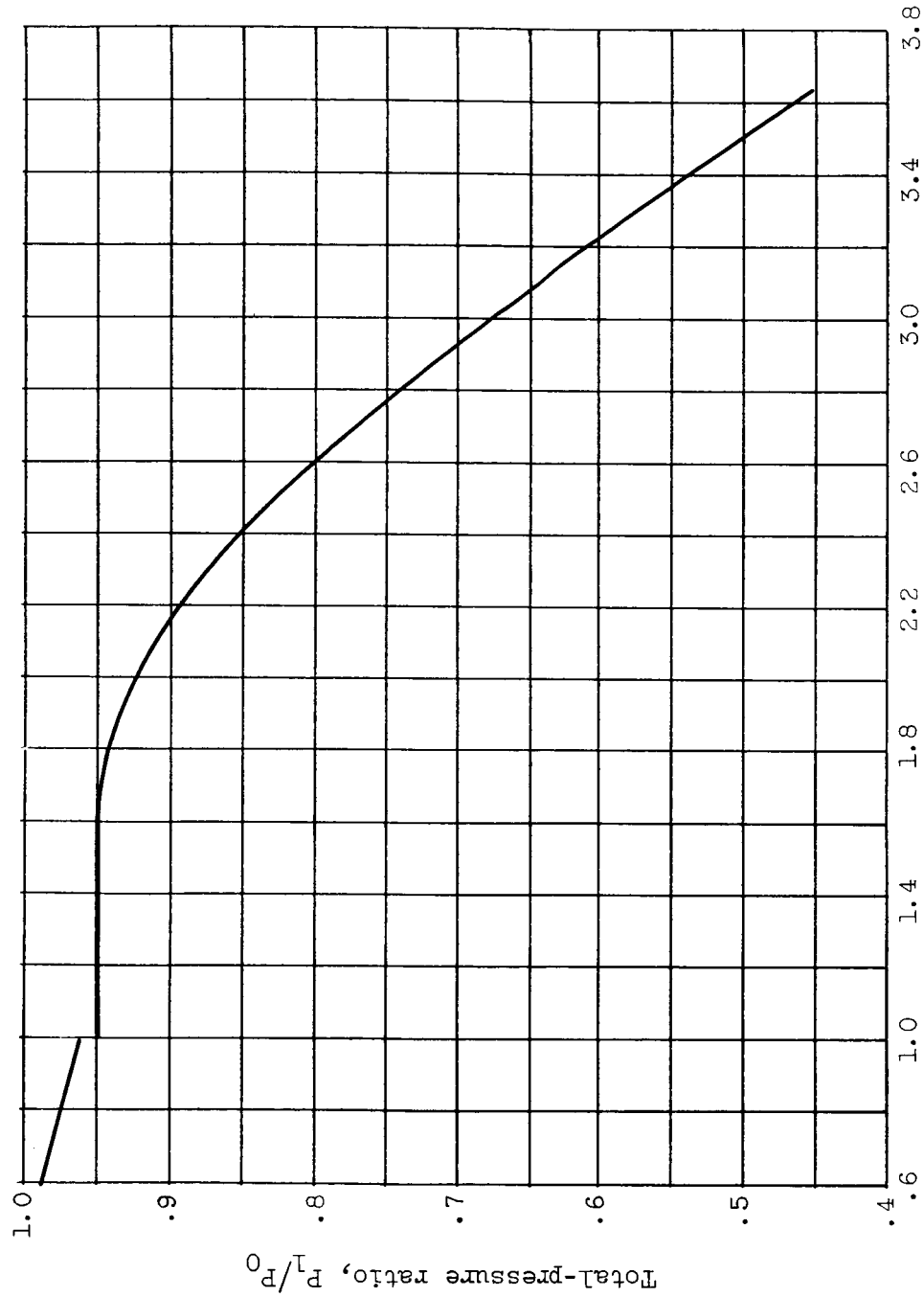

Figure 9. - Inlet-diffuser total-pressure ratio plotted against flight Mach number.

[redacted]

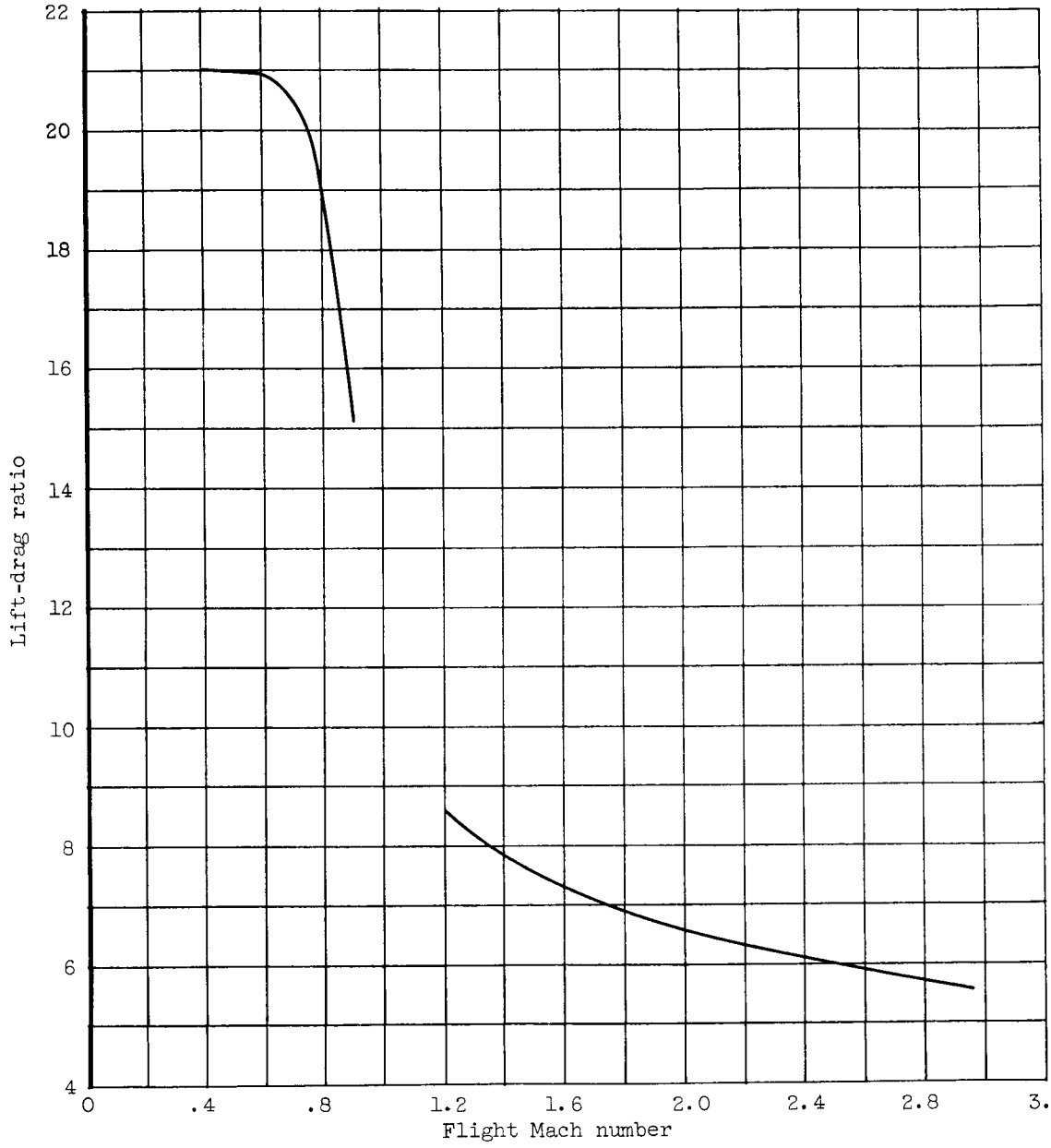

Figure 10. - Aircraft lift-drag ratio plotted against flight Mach number.

[redacted]

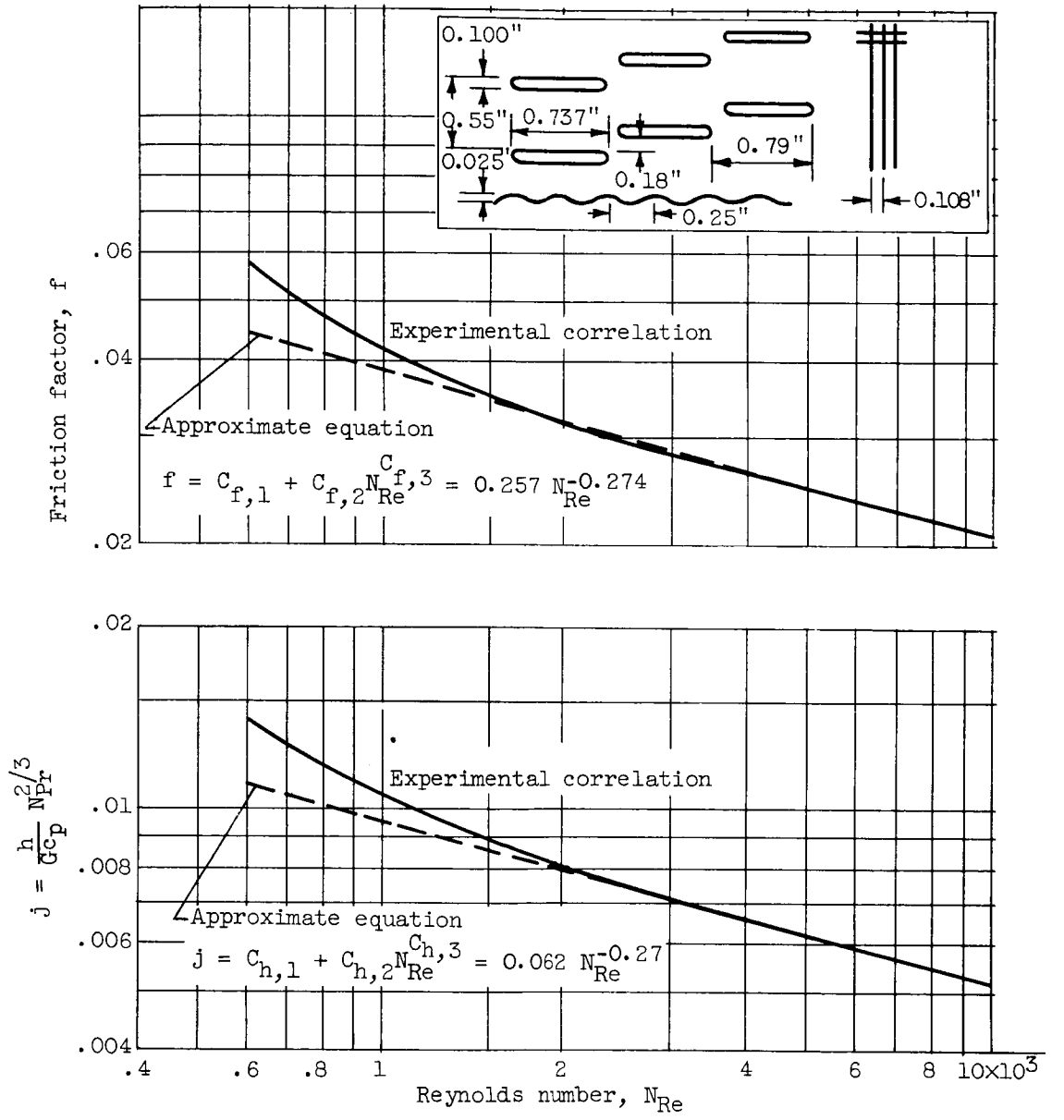

Figure 11. - Heat-exchanger geometry and performance. Finned flat tubes: fin pitch, 9.29 fins per inch; flow passage hydraulic diameter, d_e, 0.01352 foot; fin metal thickness, 0.004 inch; free-flow area/frontal area, 0.788; total heat-transfer area/total volume, 228 square feet per cubic foot; fin area/total area, 0.814.

[redacted]

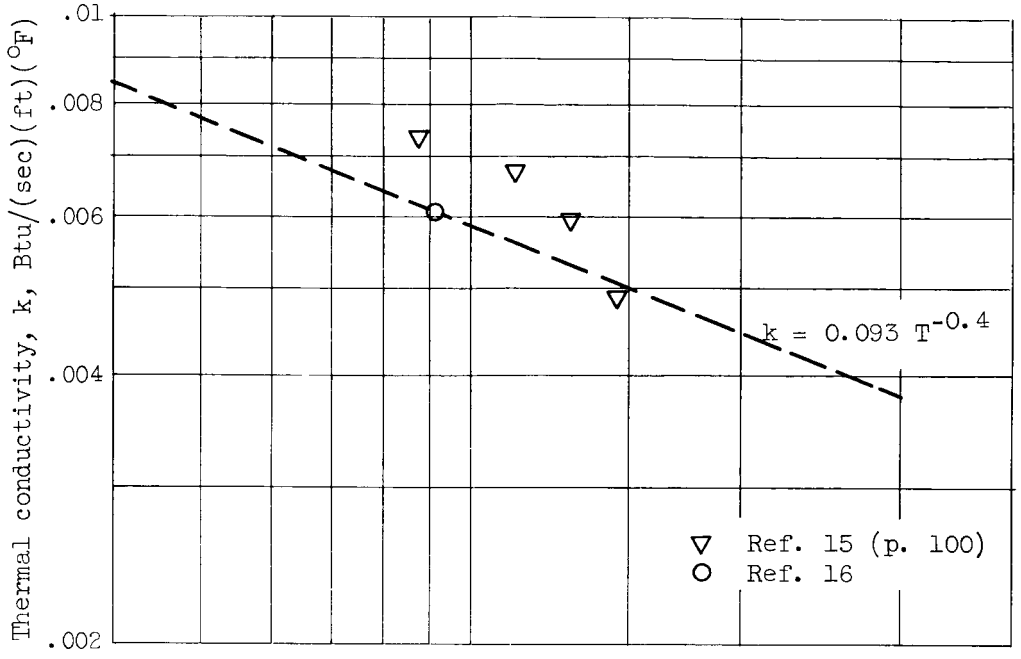

(a) Correlation of thermal conductivity with temperature.

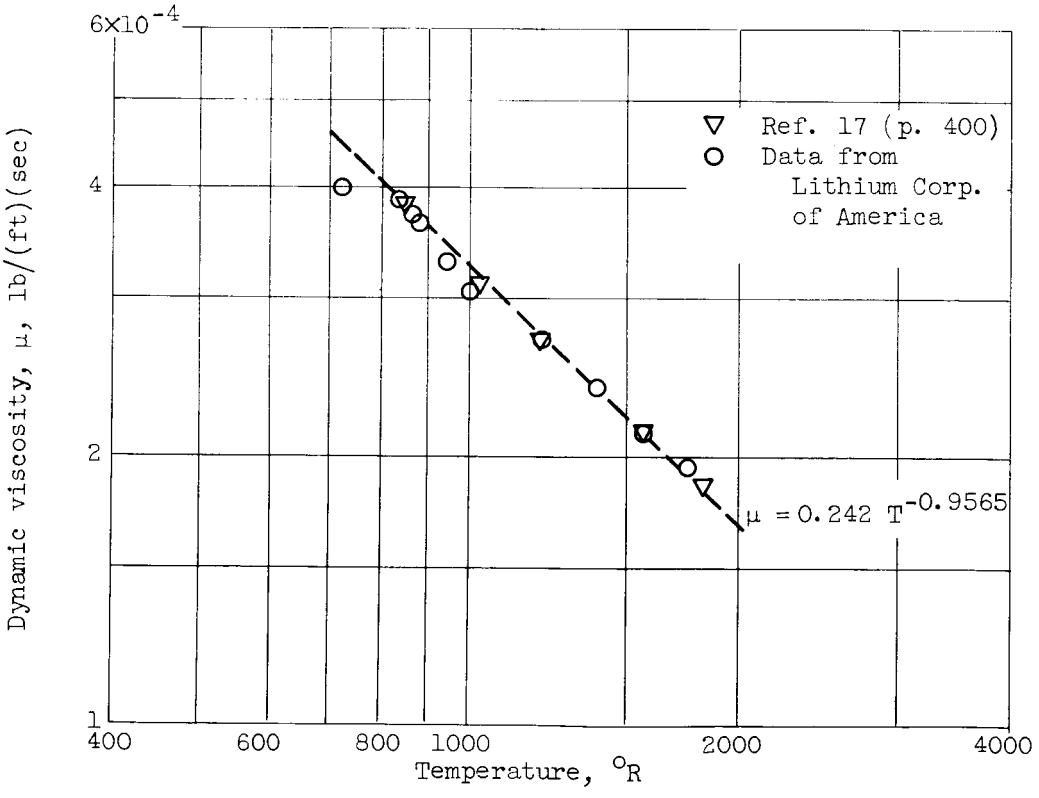

(b) Correlation of dynamic viscosity with temperature.

Figure 12. - Physical properties of lithium.

[redacted]

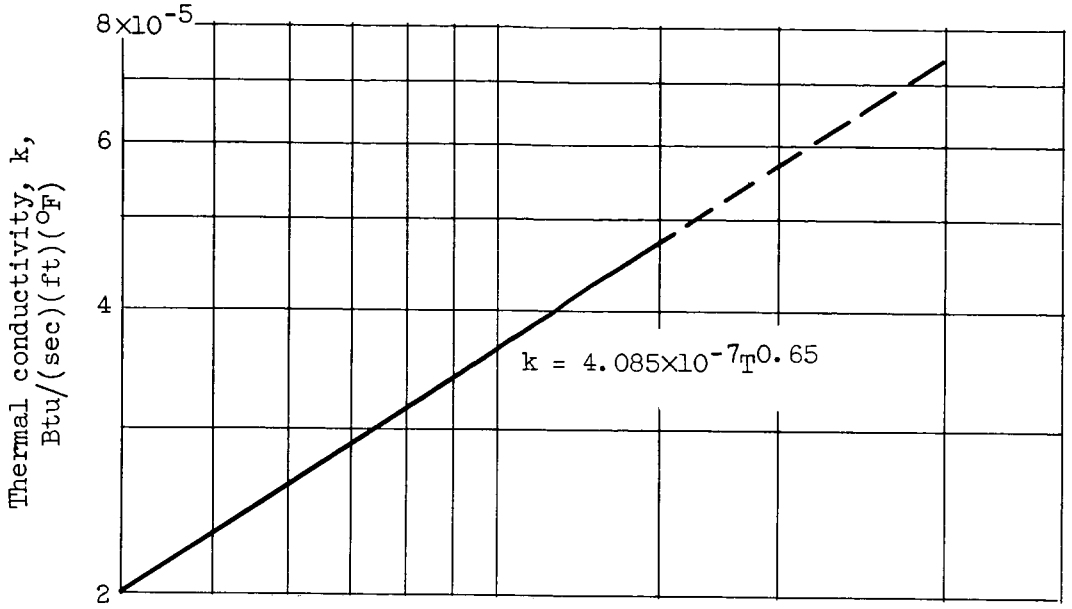

(a) Correlation of thermal conductivity with temperature.

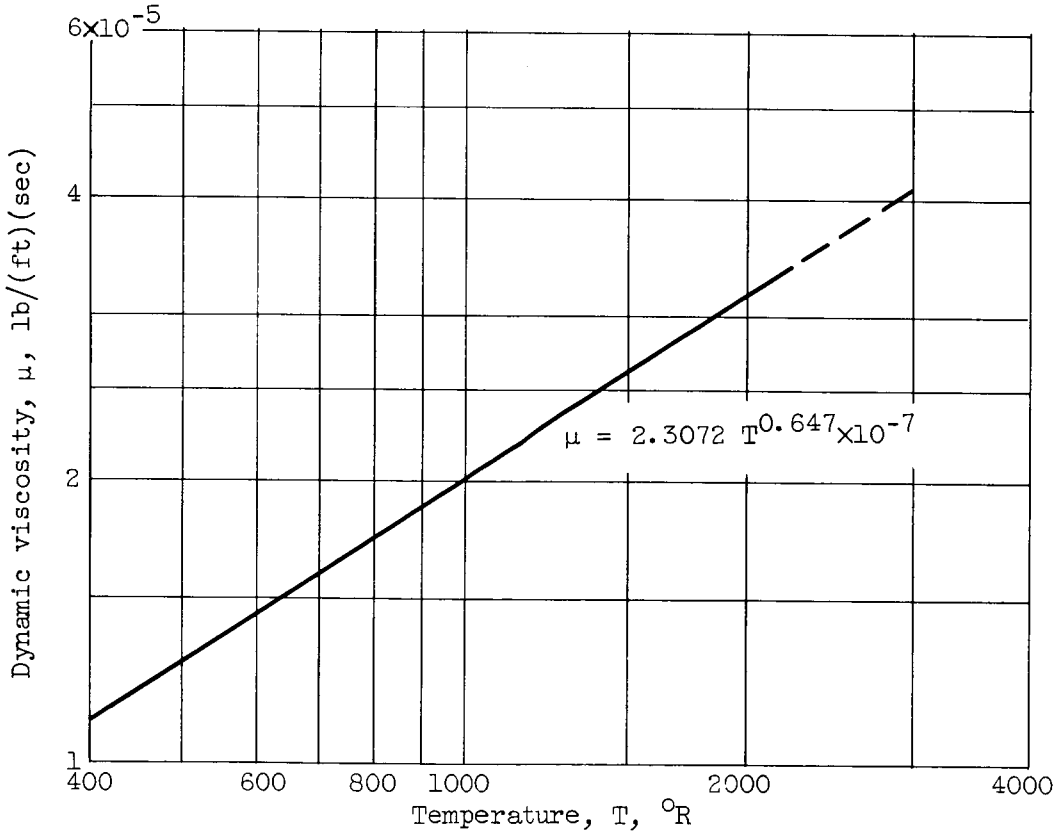

(b) Correlation of dynamic viscosity with temperature.

Figure 13. - Physical properties of helium.

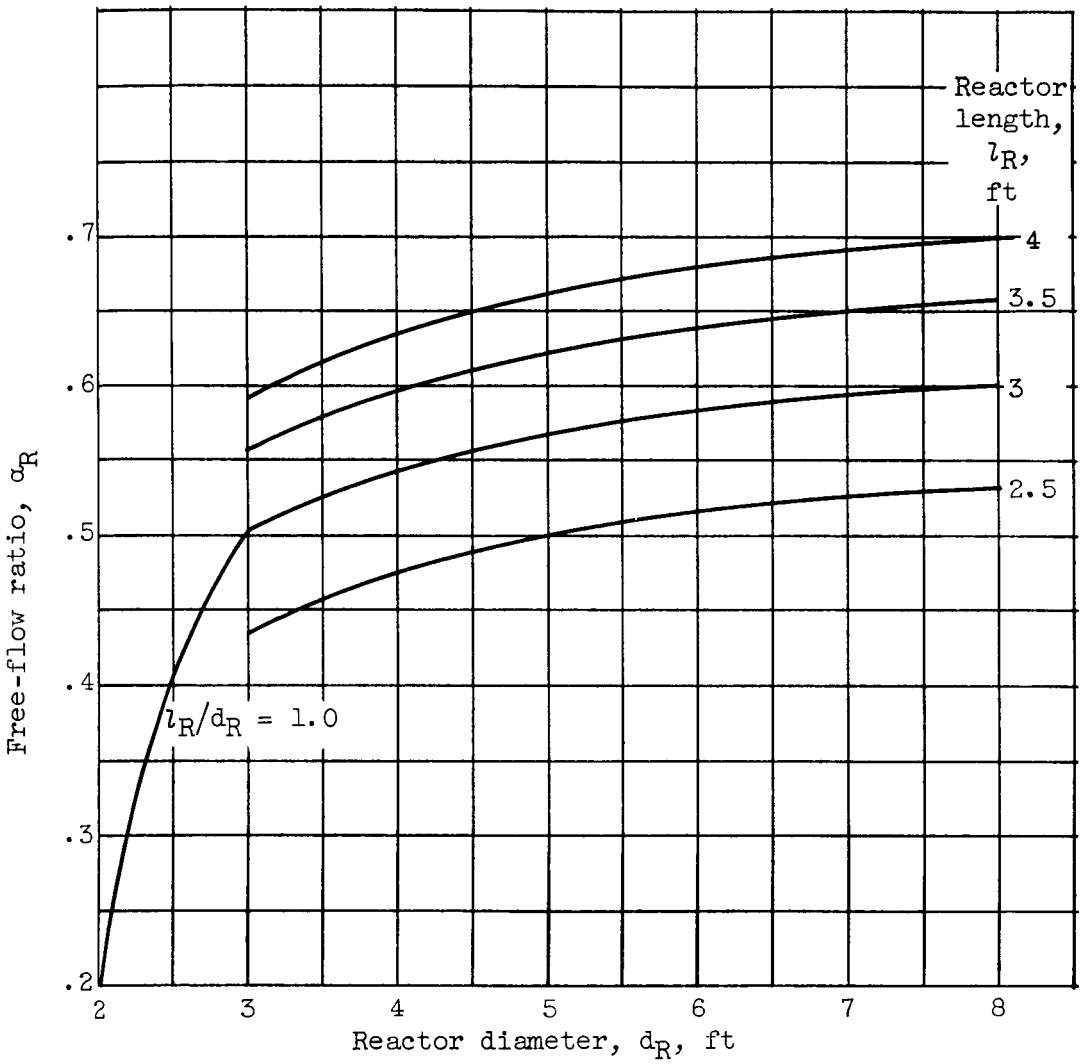

Figure 14. - Variation of reactor free-flow ratio with core diameter and length. Core, beryllium oxide, molybdenum, and uranium; 6-inch beryllium reflector; moderator-to-uranium atom ratio, 400.

E-196

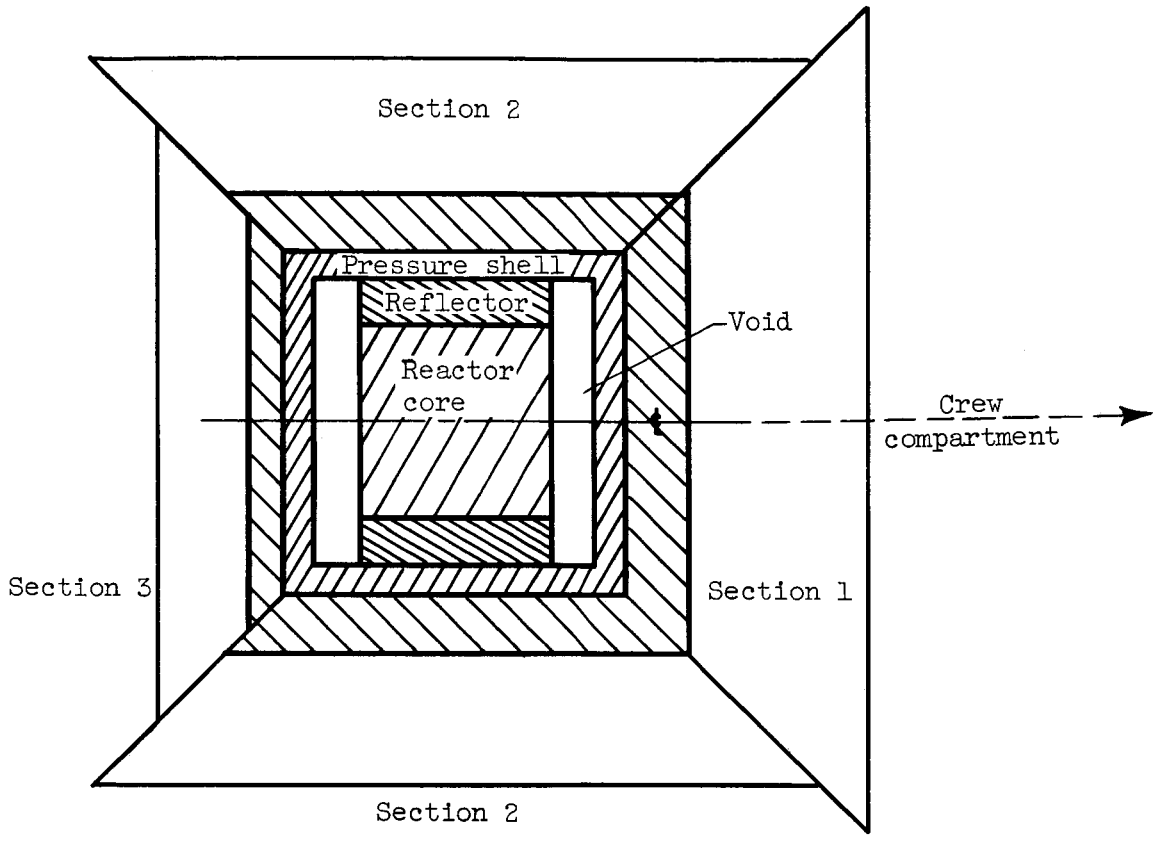

Figure 15. - Reactor-shield-assembly model for shield-weight calculation.

CONFIDENTIAL

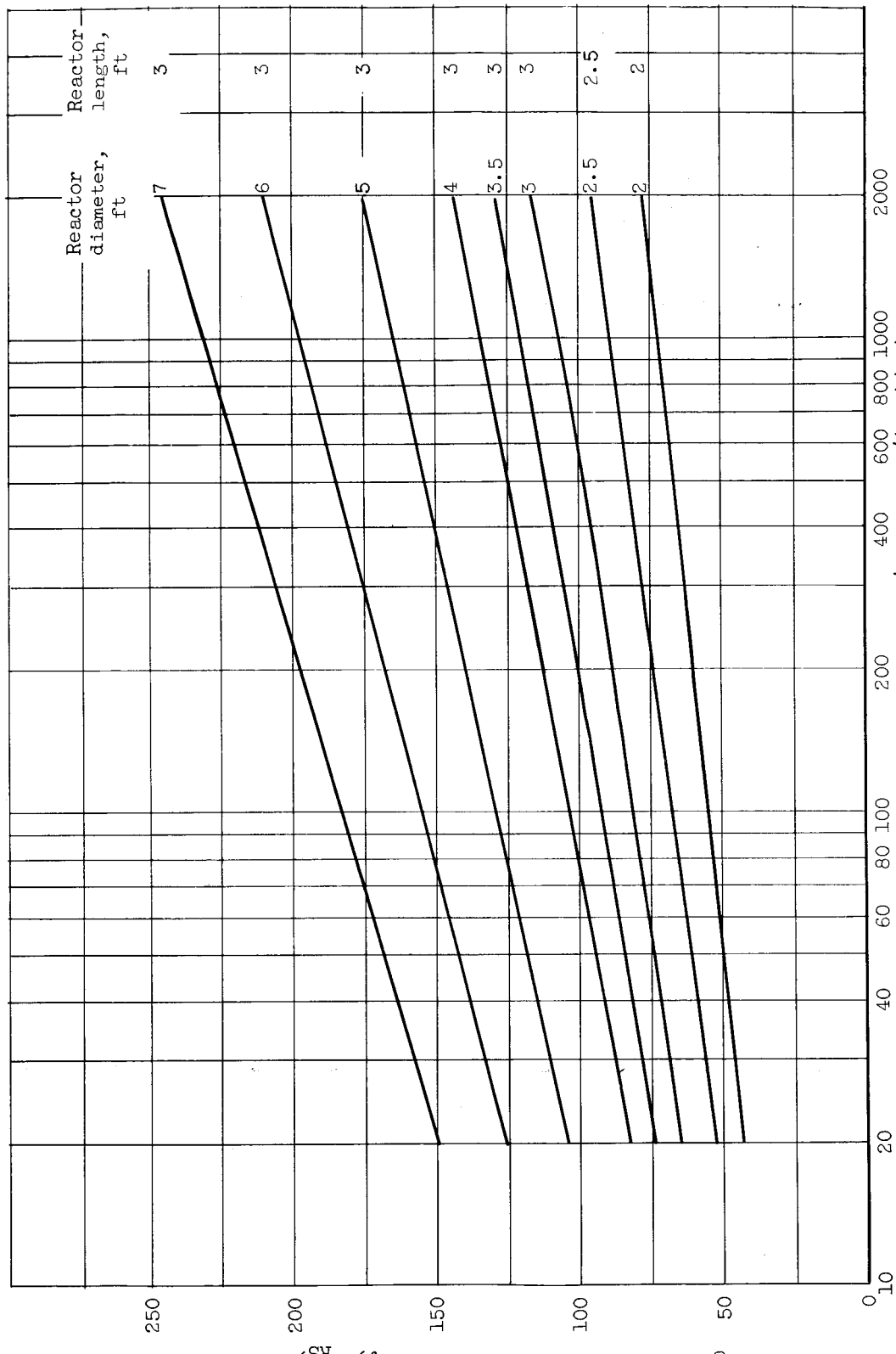

Figure 16. - Reactor-shield-assembly weight estimates. Design altitude, 35,000 feet.

CONFIDENTIAL

E-196